

The first carbon-enhanced metal-poor star found in the Sculptor dwarf spheroidal^{*}

Á. Skúladóttir¹, E. Tolstoy¹, S. Salvadori¹, V. Hill², M. Pettini³, M. D. Shetrone⁴, and E. Starkenburg⁵ ^{**}

¹ Kapteyn Astronomical Institute, University of Groningen, PO Box 800, 9700AV Groningen, the Netherlands
e-mail: asa@astro.rug.nl

² Laboratoire Lagrange, Université de Nice Sophia Antipolis, CNRS, Observatoire de la Côte d'Azur, BP 4229, 06304 Nice Cedex 4, France

³ Institute of Astronomy, Madingley Road, Cambridge CB3 0HA, England

⁴ The University of Texas at Austin, McDonald Observatory, 32 Fowlkes Rd, McDonald Observatory, Tx 79734-3005, USA

⁵ Department of Physics and Astronomy, University of Victoria, PO Box 3055, STN CSC, Victoria BC V8W 3P6, Canada

December 5, 2014

ABSTRACT

The origin of carbon-enhanced metal-poor (CEMP) stars and their possible connection with the chemical elements produced by the first stellar generation is still highly debated. In contrast to the Galactic halo, not many CEMP stars have been found in the dwarf spheroidal galaxies around the Milky Way. Here we present detailed abundances from ESO VLT/UVES high-resolution spectroscopy for ET0097, the first CEMP star found in the Sculptor dwarf spheroidal, which is one of the best studied dwarf galaxies in the Local Group. This star has $[\text{Fe}/\text{H}] = -2.03 \pm 0.10$, $[\text{C}/\text{Fe}] = 0.51 \pm 0.10$ and $[\text{N}/\text{Fe}] = 1.18 \pm 0.20$, which is the first nitrogen measurement in this galaxy. The traditional definition of CEMP stars is $[\text{C}/\text{Fe}] \geq 0.70$, but taking into account that this luminous red giant branch star has undergone mixing, it was intrinsically less nitrogen enhanced and more carbon-rich when it was formed, and so it falls under the definition of CEMP stars, as proposed by Aoki et al. (2007) to account for this effect. By making corrections for this mixing, we conclude that the star had $[\text{C}/\text{Fe}] \approx 0.8$ during its earlier evolutionary stages. Apart from the enhanced C and N abundances, ET0097 shows no peculiarities in other elements lighter than Zn, and no enhancement of the heavier neutron-capture elements (Ba, La, Ce, Nd, Sm, Eu, Dy), making this a CEMP-no star. However, the star does show signs of the weak *r*-process, with an overabundance of the lighter neutron-capture elements (Sr, Y, Zr). To explain the abundance pattern observed in ET0097, we explore the possibility that this star was enriched by primordial stars. In addition to the detailed abundances for ET0097, we present estimates and upper limits for C abundances in 85 other stars in Sculptor derived from CN molecular lines, including 11 stars with $[\text{Fe}/\text{H}] \leq -2$. Combining these limits with observations from the literature, the fraction of CEMP-no stars in Sculptor seems to be significantly lower than in the Galactic halo.

Key words. Stars: abundances – Stars: carbon – Stars: chemically peculiar – Galaxies: dwarf – Galaxies: individual (Sculptor dwarf spheroidal) – Galaxies: evolution

1. Introduction

The chemical compositions of stellar photospheres provide detailed information about the interstellar medium (ISM) from which the stars were formed. Of particular interest are the very metal-poor (VMP) stars, $[\text{Fe}/\text{H}] \leq -2$ (where $[\text{Fe}/\text{H}] = \log_{10}(N_{\text{Fe}}/N_{\text{H}})_{\star} - \log_{10}(N_{\text{Fe}}/N_{\text{H}})_{\odot}$), in the Milky Way environment, which may still preserve imprints of the first generation of stars and the early chemical evolution of the Galaxy and its surroundings. Recent surveys have revealed that a significant fraction of these low-metallicity stars in the Milky Way halo are enhanced in carbon ($[\text{C}/\text{Fe}] \geq 0.7$). The cumulative fraction of these carbon-enhanced metal-poor (CEMP) stars in the halo rises

from $\sim 20\%$ for $[\text{Fe}/\text{H}] \leq -2.5$ to $\sim 30\%$ for $[\text{Fe}/\text{H}] \leq -3.0$ and up to 75% for $[\text{Fe}/\text{H}] \leq -4.0$ (Lee et al. 2013). Including the recently discovered carbon-enhanced, hyper iron-poor star with $[\text{Fe}/\text{H}] < -7.1$ (Keller et al. 2014), the CEMP fraction at the lowest $[\text{Fe}/\text{H}]$ becomes even higher.

Traditionally, CEMP stars are categorized by their heavy element abundance patterns. Some are enriched in heavy neutron-capture elements built by the slow-process (such as Ba) and are labeled CEMP-*s* stars, and those that show significant abundances of heavy elements from the rapid-process (such as Eu) are referred to as CEMP-*r* stars. Those that show enhancements of elements from both processes are labeled CEMP-*s/r* stars. Finally, CEMP-no stars show no enhancements of the main *r*- or *s*-process elements.

The main *s*-process happens in low mass ($M \lesssim 4 M_{\odot}$) asymptotic giant branch (AGB) stars, while the *r*-process requires a high energy, neutron-rich environment, so sites such as supernovae (e.g., Travaglio et al. 2004) and neu-

^{*} Based on observations made with ESO telescopes at the La Silla Paranal observatory under program IDs 291.B-5036 (director's discretionary time) and 089.B-0304(B)

^{**} CIFAR Global Scholar

Table 1. UVES Observations of ET0097.

R.A.	Dec.	v_r (km s $^{-1}$)	Obs. date	Exp.time (min)	Airmass (start)	Airmass (end)	Seeing
00 ^h 59 ^m 12 ^s	−33°46′21″	108.97 ± 0.32	2013-08-17	47.65	1.014	1.042	0.71
			2013-09-01	47.65	1.129	1.261	1.04
			2013-09-04	47.65	1.179	1.080	0.79
			2013-09-04	47.65	1.068	1.023	0.85

tron star mergers (Tsujiyama & Shigeo 2014) have been proposed. The lighter neutron-capture elements (such as Sr, Y and Zr) are created in the main r -process, but are overabundant at lower [Fe/H] compared to the heavier r -process elements, so an extra source, the weak r -process or the weak s -process, is needed to explain the observed abundances (Travaglio et al. 2004; François et al. 2007; Frischknecht et al. 2012; Cescutti & Chiappini 2014).

In general, CEMP- s and CEMP- s/r stars have abundance patterns that suggest mass transfer from a companion in the AGB phase (Lucatello et al. 2005). Thus the C, N, O, and heavy elements for these stars do not reflect the ISM from which they were formed. The available data for CEMP- s stars is consistent with $\sim 100\%$ binary fraction and a maximum period of $\sim 20,000$ days (Starkenburger et al. 2014).

CEMP-no stars, however, are not especially associated with binaries. Though some of them do belong to binary systems, for many of them close binaries that favor mass transfer can be excluded (e.g., Starkenburg et al. 2014). These stars are more frequent, and their carbon enhancement becomes more extreme at lower [Fe/H] (e.g., Lee et al. 2013; Norris et al. 2013), so it is difficult to explain the abundance pattern of such stars with mass transfer from an AGB-companion. Though other scenarios have been discussed, CEMP-no stars are generally believed to have formed out of carbon-enhanced gas clouds, enriched by low- and/or zero-metallicity stars. Thus, CEMP-no stars could provide direct information on the properties of the first generation of stars.

Among the proposed sources of C-enrichment in CEMP-no stars (see Norris et al. 2013 for a detailed overview), two are of particular interest: (i) massive rapidly rotating zero-metallicity stars that produce large amounts of C, N, and O due to distinctive internal burning and mixing episodes (Meynet et al. 2006); (ii) faint SNe, associated with the first generations of stars, which experience mixing and fallback, ejecting large amounts of C but small amounts of Fe and the other heavier elements (Umeda & Nomoto 2003; Iwamoto et al. 2005; Tominaga et al. 2007).

Most of the observed CEMP stars have been found in the Galactic halo and a few have been found in the ultra faint (UF) galaxies around the Milky Way. Two stars with very high carbon values ($[C/Fe] > 2$) have been found in the UF galaxies Bootes (Lai et al. 2011) and Segue I (Norris et al. 2013). No star with $[C/Fe] > 2$ has been found in the more luminous ($L_{\text{tot}} > 10^5 L_{\odot}$), more distant dwarf spheroidal (dSph) galaxies, but some CEMP stars with lower carbon abundances have been observed, such as a star in Sextans dSph with $[C/Fe] \sim 1$ at $[Fe/H] \sim -3$ (Honda et al. 2011). In particular, no VMP star has been found in the Sculptor dSph with $[C/Fe] > 0.1$ until now, despite extensive searches for low-metallicity stars (e.g., Tafelmeyer et al. 2010; Starkenburg et al. 2013).

Sculptor is a well-studied system with a magnitude of $M_V \approx -11.2$ and a distance of 86 ± 5 kpc (Pietrzyński et al. 2008). It is at high Galactic latitude ($b = -83^\circ$) and has systemic velocity of $v_{\text{hel}} = +110.6 \pm 0.5$ km/s. The contamination by foreground Galactic stars is not significant, and most of it can be easily distinguished by velocity (e.g., Battaglia et al. 2008). The star formation history shows a peak in star formation ~ 13 Gyr ago, with a slow decrease, so the galaxy is dominated by an old stellar population (> 10 Gyr old), and has not formed any stars for the last ~ 6 Gyr (de Boer et al. 2012).

Large spectroscopic surveys of individual stars have been carried out in the central field of Sculptor. Abundances have been measured for Fe, Mg, Ca, Si, and Ti with intermediate-resolution (IR) spectroscopy (Kirby et al. 2009) and high-resolution (HR) spectroscopy for ~ 100 stars (Dwarf Abundances & Radial-velocities Team (DART) survey, Tolstoy et al. 2009; Hill et al. in prep.). Because of the distance to Sculptor, in general only the brightest stars of the galaxy are available for HR spectroscopy. The HR sample is therefore mostly limited to the upper part of the red giant branch (RGB) ($0 \lesssim \log g \lesssim 2$). None of the large surveys of Sculptor have included measurements of carbon abundances, but several follow-up spectra of low-metallicity stars have been taken, many of them including C measurements (Tafelmeyer et al. 2010; Frebel et al. 2010; Kirby & Cohen 2012; Starkenburg et al. 2013).

In addition, there have been surveys of Carbon-stars and CH-stars in Sculptor (e.g., Azzopardi et al. 1986), some of which that have been followed up with IR spectra (e.g., Groenewegen et al. 2009). The carbon-enhancement of these stars is believed to come from internal processes or mass transfer, and does not reflect the ISM from which they were formed. Thus they will not be discussed further in this paper.

The star ET0097 is thus the most inherently carbon-rich star in the Sculptor dSph measured to date, with $[Fe/H] = -2.03 \pm 0.10$ and $[C/Fe] = 0.51 \pm 0.10$. It was even more carbon-enhanced in the past, with $[C/Fe] \approx 0.8$, making it the first CEMP observed in Sculptor. A detailed chemical analysis of this star is presented here, from an HR spectrum observed with the VLT/UVES telescope at the European Southern Observatory (ESO). In addition, carbon abundance estimates and upper limits for 85 other stars are presented, derived from CN molecular lines in the wavelength range 9100–9250 Å, from VLT/FLAMES spectra.

2. Observations and data reduction

From the DART survey (Tolstoy et al. 2006), detailed abundance measurements are known for ~ 100 stars, spread over a $25'$ diameter field of view in the Sculptor dSph (Hill et al. in prep.; Tolstoy et al. 2009). As a part of this project, ESO VLT/FLAMES/GIRAFFE HR spectroscopy

Table 2. Signal-to-noise ratios of the different parts of the final coadded spectrum.

Wavelength range (Å)	S/N
3770-4980	30
5760-7510	50
7660-9450	50

was carried out over the wavelength range $\sim 9100\text{-}9300$ Å, to measure S abundances in Sculptor (Skúladóttir et al. in prep.). In most of these spectra CN molecular lines were observed, with the exception of the most metal-poor stars ($[\text{Fe}/\text{H}] \lesssim -2.2$). This CN molecular band was exceptionally strong in the star ET0097 and to follow up that observation, an HR spectrum over a long wavelength range was taken for the star, using ESO VLT/UVES.

UVES is a dichroic HR optical spectrograph at the VLT (Dekker et al. 2000), where the light beam from the telescope can be split into two arms, the Ultra Violet to the Blue arm and the Visual to the Red arm. The observations were taken in August and September of 2013, using a 1.2" slit, with a resolution of 40,000 in the blue, and 35,000 in the red. The observational details are listed in Table 1.

The details regarding the observations and data reduction for the VLT/FLAMES data, along with the S measurements will be presented in an upcoming paper, Skúladóttir et al. in prep.

2.1. Data reduction

The ESO VLT/UVES spectrum was reduced, extracted, wavelength calibrated, and sky-subtracted using the UVES pipeline provided by ESO (Freudling et al. 2013). The reduced spectra were corrected for telluric absorption using spectra of a blue horizontal branch star, taken the same nights as the observations. The spectra taken at different times all showed comparable counts, so they were combined using a median value of the four spectra. The usable wavelength range and their relative signal-to-noise (S/N) ratios are listed in Table 2. The S/N ratios were evaluated as the mean value over the standard deviation of the continuum in line-free regions.

2.2. Continuum normalization

In the red part of the spectrum ($\sim 5800\text{-}9400$ Å), the entire wavelength range was covered with CN molecular lines, most of them weak, but some stronger. To find proper continuum points for the spectrum, a synthetic spectrum was made, using rough estimates of the oxygen, carbon, and nitrogen abundances. An iterative comparison with the normalized observed spectrum was then used to find a better synthetic spectrum, which was used for a better determination of continuum points. This process was iterated until the result was stable.

A similar approach was used for the reddest part of the blue spectrum ($\sim 4500\text{-}5000$ Å) that is covered in relatively weak CH and C₂ molecular lines. For the bluer part of the spectrum, true continuum points became rarer, and a continuum could only be estimated from points close to the continuum. At the bluest part of the spectrum, the B-X band of CN at 3888 Å is extremely strong, and wipes out all continuum points making normalization in the region very

Table 3. Photometry of ET0097.

Colour	mag.	err	E(V-X)	T_{eff} (K)
V	17.255	0.002		
V-I	1.246	0.005	0.023	4382
V-J	2.125	0.004	0.041	4393
V-K	2.954	0.005	0.050	4378

uncertain, so the bluest part of the spectrum ($\lesssim 3900$ Å) could not be used in the abundance analysis.

Where enough continuum points were available, the spectrum was also renormalized around each line being measured by a constant factor for better accuracy, but this change in the height of the continuum was minimal, rarely more than 1-2%.

3. Stellar parameters

The photometry for ET0097 comes from deep wide field imaging in the V and I bands (de Boer et al. 2011) and the infrared photometry, bands J and K, come from VISTA survey observations, see Table 3. Although photometry is also available for the B band, it was not used, since in this carbon-rich star it is affected by the strong CH molecular band in the region.

The effective temperature of the star, T_{eff} , was determined from the photometry following the recipe from Ramírez & Meléndez (2005) for giants with metallicity $[\text{Fe}/\text{H}] = -2.02$ and assuming a reddening correction, $E(V-X)$, in the direction of the Sculptor dSph as evaluated by Schlegel et al. (1998), see Table 3. The result, $T_{\text{eff}} = 4383 \pm 35$ K, is 83 K higher than the temperature adopted for this star in Hill et al. in prep., but agrees within the error bars. Included in the estimated errors are the $\sigma(T_{\text{eff}})$ provided by Ramírez & Meléndez (2005) for each color used, the photometric errors and the (minor) effect of the observational errors of $[\text{Fe}/\text{H}]$.

The surface gravity for the star is obtained using the standard relation:

$$\log g_{\star} = \log g_{\odot} + \log \frac{M_{\star}}{M_{\odot}} + 4 \log \frac{T_{\text{eff},\star}}{T_{\text{eff},\odot}} + 0.4(M_{\text{bol},\star} - M_{\text{bol},\odot}) \quad (1)$$

which yields the surface gravity $\log g_{\star} = 0.75 \pm 0.13$.

The absolute bolometric magnitude for the star, $M_{\text{bol},\star} = -3.01 \pm 0.08$, is calculated using a calibration for the V-band magnitude (Alonso et al. 1999) and a distance modulus of $(m - M)_{\odot} = 19.68 \pm 0.08$, from Pietrzyński et al. (2008), which dominates the error on $M_{\text{bol},\star}$, as the photometric errors are negligible. The mass of the star is assumed to be $M_{\star} = 0.8 \pm 0.2 M_{\odot}$. The solar values used are the following: $\log g_{\odot} = 4.44$, $T_{\text{eff},\odot} = 5790$ K and $M_{\text{bol},\odot} = 4.72$.

The microturbulence velocity, v_t , was spectroscopically derived by making sure the abundance measurements for Fe I do not show a trend with the equivalent width, $\log(EW/\lambda)$. The result is $v_t = 2.25 \pm 0.20$ km/s.

No significant slope was found between the iron abundances of individual lines and their relevant wavelength or their excitation potential, confirming the validity of the determined stellar parameters.

Table 5. Element abundances of ET0097. [Fe I/H] is adopted as the reference iron value [Fe/H]. For other elements the adopted value is an average of all lines available, in some cases more than one ionization stage, see Table 4 for details. No corrections have been made for NLTE effects. The solar values are adopted from Grevesse & Sauval (1998).

X	$\log \epsilon_{\odot}$	N_X	$\log \epsilon$	[X/Fe]	δ_{noise}	δ_{total}
Fe I	7.50	49	5.47	-2.03 ^a	0.02	0.10
Fe II	7.50	4	5.64	-1.86 ^a	0.10	0.14
Li	1.10	1	< 0.17	< 1.10	-	-
C	8.52	-	7.00	0.51	0.09	0.10
N	7.92	-	7.07	1.18	0.20	0.20
O	8.83	2	7.33	0.53	0.18	0.19
Na	6.33	3	3.81	-0.49	0.24	0.24
Mg	7.58	5	5.97	0.42	0.04	0.06
Al	6.47	1	3.62	-0.82	0.80	0.80
Si	7.55	7	5.77	0.25	0.09	0.11
S	7.33	2	5.44	0.14	0.29	0.29
K	5.12	2	3.45	0.36	0.07	0.08
Ca	6.36	20	4.49	0.16	0.02	0.04
Sc	3.17	9	1.10	-0.04	0.04	0.06
Ti	5.02	35	3.12	0.13	0.02	0.07
V	4.00	10	2.01	0.04	0.04	0.06
Cr	5.67	16	3.53	-0.11	0.07	0.08
Mn	5.39	9	3.13	-0.23	0.06	0.07
Co	4.92	7	2.92	0.03	0.10	0.11
Ni	6.25	22	4.18	-0.04	0.04	0.07
Cu	4.21	1	1.44	-0.74	0.26	0.26
Zn	4.60	3	2.68	0.11	0.23	0.23
Ga	2.88	1	0.82	-0.03	0.44	0.44
Sr	2.97	2	1.65	0.71	0.20	0.20
Y	2.24	6	0.55	0.34	0.04	0.06
Zr	2.60	5	0.94	0.37	0.06	0.07
Ba	2.13	5	-0.34	-0.44	0.06	0.08
La	1.17	10	-1.08	-0.22	0.09	0.09
Ce	1.58	8	-0.62	-0.17	0.12	0.13
Pr	0.71	1	< -1.10	< 0.22	-	-
Nd	1.50	10	-0.61	-0.08	0.05	0.07
Sm	1.01	3	-0.91	0.11	0.32	0.32
Eu	0.51	4	-1.49	0.03	0.42	0.42
Gd	1.12	1	< -0.50	< 0.41	-	-
Tb	0.35	1	< -1.38	< 0.30	-	-
Dy	1.14	2	-0.92	-0.03	0.53	0.53
Er	0.93	1	< -0.60	< 0.50	-	-
Pb	1.95	1	< 0.92	< 1.00	-	-
Th	0.09	1	< -1.20	< 0.74	-	-

^a[Fe/H]

4. Abundance measurements

All analysis was carried out using the spectral synthesis code TURBOSPEC developed by Bernard Plez (Alvarez & Plez 1998; Plez 2012). Because of the evolutionary stage of ET0097, its relatively low temperature and its high C and N abundances, most of the observed wavelength range is covered with CN and/or CH molecular lines. Synthetic spectra are therefore necessary to include the effects of these lines in the abundance evaluation and to distinguish between lines with different degrees of blending. The line list used was chosen to minimize the use of heavily blended lines, and when possible only lines with minimal or no blending were used (see Table 4).

The stellar atmosphere models are adopted from MARCS (Gustafsson et al. 2008) for stars with standard composition, 1D and assuming local thermodynamic equilibrium (LTE), interpolated to match the exact stellar parameters for ET0097. Parameters for the atomic lines are adopted from the DREAM data base (Biémont et al. 1999), extracted via VALD (Kupka et al. 1999 and references therein). The molecular parameters for C₂ come from M. Querci (private communication), and are described in Querci et al. (1972). For CH molecular lines, we use the data from Plez et al. (2007). The molecular parameters for CN are from T. Masseron (private communication), derived with similar methods and lab data as Brooke et al. (2014) and Sneden et al. (2014).

The results of the abundance analysis are listed in Table 5. To maintain consistency with Hill et al. (in prep.), the solar values used are from Grevesse & Sauval (1998), and where data from the literature is included, it is shifted to match this scale.

4.1. Iron

Special care was taken to ensure that the measured Fe lines were not severely blended with CN, C₂, or CH molecular lines. Only Fe I lines that changed by less than 0.1 dex, when both the assumed carbon and nitrogen abundances were either increased or decreased by 0.2 dex, were used. Increasing both elements by this value had a strong effect on the CN line strength, so the real effect from the uncertainty on C and N abundance measurements should be much less than 0.1 dex on the selected Fe I lines and, in all cases, it is less than the statistical errors on the individual lines. In total, 49 Fe I lines could be used in the wavelength range 5600-9200 Å, see Table 4. All Fe I lines in the bluer part of the spectrum were too blended to comply with the rather strict criteria for unblended lines.

For Fe II, no lines were found that fulfill the criteria, so the four least blended Fe II lines were used for the measurement.

4.2. Oxygen, carbon, and nitrogen

The oxygen abundance was derived from the forbidden [O I] lines at 6300 and 6364 Å, see Fig. 1. Both lines were slightly blended with weak CN molecular lines, but changing the adopted C and N values by ± 0.20 around the best fit, changed the measured oxygen abundances only by ~ 0.05 dex. The abundance measurements of the lines agree within the errorbars, $\log \epsilon(\text{O})_{6300\text{\AA}} = 7.30 \pm 0.14$ and $\log \epsilon(\text{O})_{6364\text{\AA}} = 7.46 \pm 0.30$. The final value of $\log \epsilon(\text{O}) = 7.33 \pm 0.18$ was adopted by weighting the two [O I] lines with their errors.

The [O I] lines of the triplet at 7774 Å were too weak to be accurately measured, considering the noise and slight blending, and they were therefore not included in the measurement.

The carbon abundance for ET0097 was determined by fitting three different molecular bands in regions of 20 Å. Parts of these bands are shown in Fig. 2. In some wavelength ranges, the molecular lines were saturated and in others very weak. Therefore, we only used regions where the χ^2 of the fit was sensitive to the assumed C abundance. The CH G-band at ~ 4300 Å, spreading throughout the

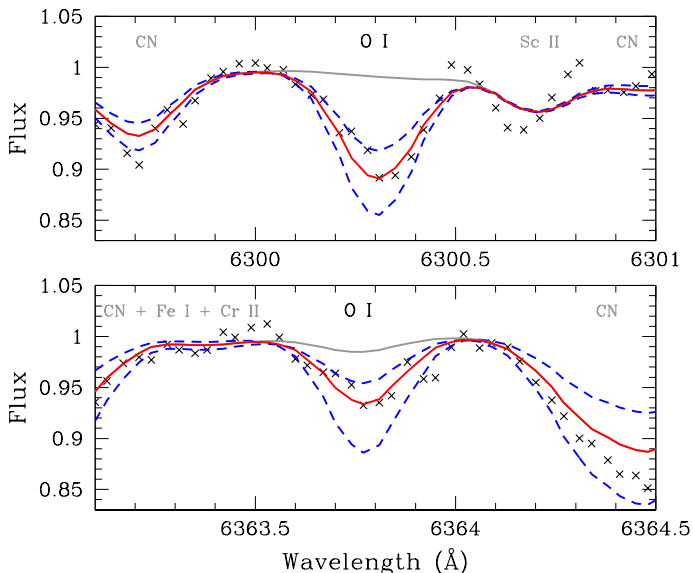


Fig. 1. Measured oxygen lines, $\log \epsilon(\text{O})_{6300\text{\AA}} = 7.30 \pm 0.14$ and $\log \epsilon(\text{O})_{6364\text{\AA}} = 7.46 \pm 0.30$. Solid red lines show best fits, and dashed blue lines show upper and lower limits of error bars. Cases where [O I] lines have been removed from the linelist are shown with solid gray lines. The strength of CN molecular lines is very sensitive to oxygen abundance. Adopting a lower O abundance will make CN lines in the synthetic spectrum stronger, assuming fixed values of C and N.

range $\sim 4200\text{--}4400\text{\AA}$, resulted in $\log \epsilon(\text{C})_{\text{CH:4300}\text{\AA}} = 6.98$. The C_2 band around $\sim 4700\text{\AA}$ gave a result 0.20 dex lower, $\log \epsilon(\text{C})_{\text{C}_2:4700\text{\AA}} = 6.78$. A relatively weak CH band (A-X system) at $\sim 4850\text{\AA}$ was also used to measure carbon, yielding a value 0.25 dex higher than the stronger CH-band, $\log \epsilon(\text{C})_{\text{CH:4850}\text{\AA}} = 7.23$. The final measured value of $\log \epsilon(\text{C}) = 7.00 \pm 0.10$ was adopted by averaging both CH bands and the C_2 band, weighting them with the size of the region available for the measurements.

The CN band at 4215\AA (B-X system) appeared clearly and without severe saturation (see Fig. 3). A big portion of the observed spectrum for ET0097 was covered with CN lines, due to the relatively low temperature of the star and the high C and N abundances. The nitrogen was therefore measured using both the band at 4215\AA and CN molecular lines in the wavelength range $\sim 6200\text{--}9400\text{\AA}$ (A-X system), giving the final result of $\log \epsilon(\text{N}) = 7.07 \pm 0.20$. Regions where the χ^2 of the fit was insensitive to the nitrogen abundance were excluded. The nitrogen measurements, which cover 104 regions of 20\AA , show no trend with wavelength and are very consistent with a low scatter, $\sigma = 0.05$. The measurements in the redder part of the spectrum and the CN band at 4215\AA are in perfect agreement, see Fig. 3, indicating that the CN molecular parameters in the red are reliable. The uncertainty in the measurement from the CN band in the blue is higher than in the red, mostly due to the uncertain continuum determination. Using the larger wavelength range, however, the statistical errors for the nitrogen become negligible, and the real uncertainties come from errors in the carbon and oxygen measurements.

The B-X system of CN at 3888\AA was extremely strong in this star and wiped out all continuum points until the bluest end of the spectrum at $\sim 3770\text{\AA}$. Thus, it was not included in the abundance measurement of nitrogen. However, as far as rough continuum estimation allowed, it was

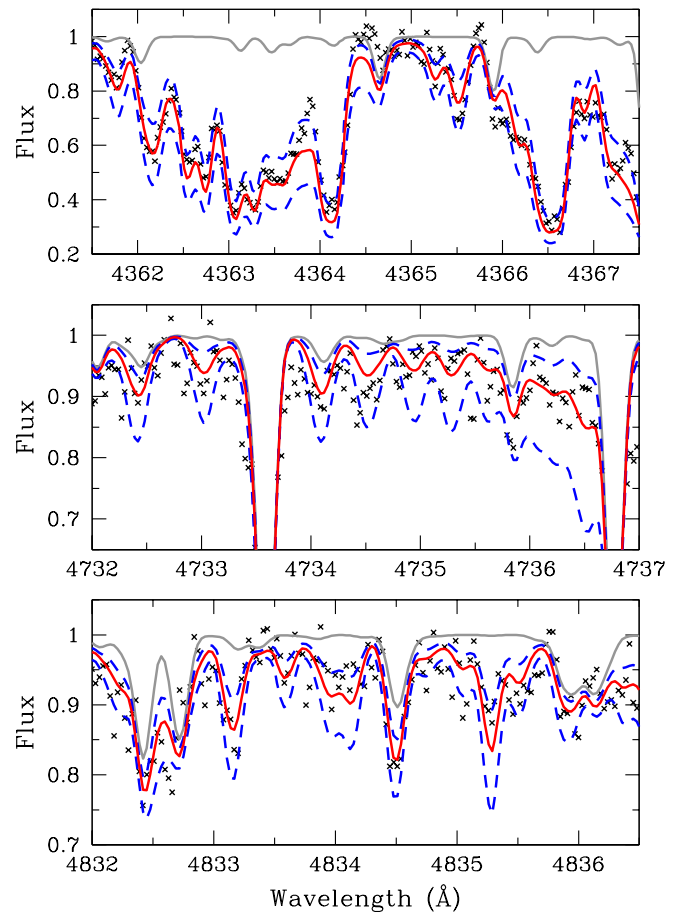


Fig. 2. Spectra of different regions used for the measurement of carbon. Top panel shows part of the CH region at $\sim 4300\text{\AA}$ (G-band), middle panel shows the C_2 band, and lowest panel shows the CH band (A-X system) at $\sim 4850\text{\AA}$. In all cases, solid red lines show best fits of the regions (as listed in the text), dashed blue lines show carbon values ± 0.20 from that fit, and solid gray lines show how the spectrum would look without any carbon. Note that the scale on the y-axis is not the same for all panels.

consistent with the result obtained using the other CN molecular bands.

Because CO locks away a sizable fraction of the C available in the star, both CH bands and the C_2 band are sensitive to the oxygen value, and the nitrogen abundance measured from the CN molecular bands is sensitive both to the oxygen and the carbon abundances. Therefore, the oxygen-carbon-nitrogen measurements were iterated several times to minimize the influence of the errors of one element on the other elements as much as possible.

4.3. Indicators of mixing, $^{12}\text{C}/^{13}\text{C}$ ratio and Li

When a star moves along the RGB, it undergoes a second episode of mixing (at the so-called RGB-bump) that lowers the carbon abundance at its surface, and increases the nitrogen. This upper RGB phase is reached at the luminosity $\log L_*/L_\odot \sim 2.2$, for stars in the metallicity range $-2.0 \lesssim [\text{Fe}/\text{H}] \lesssim -1.0$ (Gratton et al. 2000) and when $\log L_*/L_\odot \sim 2.6$ for $[\text{Fe}/\text{H}] \lesssim -2.5$ (Spite et al. 2006). Before an RGB star reaches this high luminosity, its C and

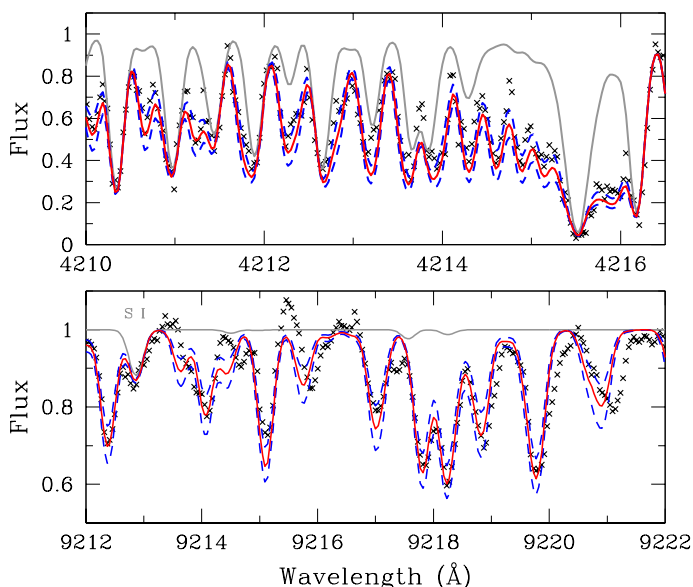


Fig. 3. Upper panel shows strong CN molecular band at 4215 Å (B-X system), while lower panel shows an example of the CN molecular band seen in the redder part of the spectrum. In both cases, solid red lines show the best fit of $\log \epsilon(\text{N}) = 7.07$, dashed blue lines show nitrogen values ± 0.20 from that fit, and solid gray lines what the spectrum would look like without any molecular CN lines. Note that the scale on the y-axis is not the same for both panels.

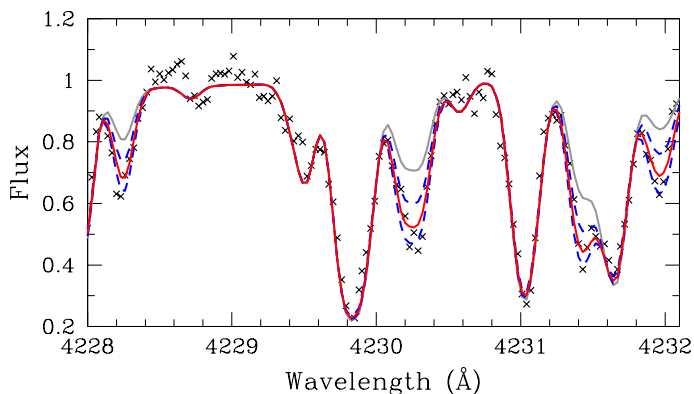


Fig. 4. Example of the ^{13}C features used for evaluating the $^{12}\text{C}/^{13}\text{C}$ isotope ratio. Solid gray line shows the synthetic spectrum assuming $\log^{12}\text{C}/^{13}\text{C} = 1.3$, value typical for unmixed giants (Spite et al. 2006), solid red line shows $\log^{12}\text{C}/^{13}\text{C} = 0.8$, and dashed blue lines show ratios ± 0.2 from that value.

N abundances do not change significantly during the star’s evolution (Gratton et al. 2000).

Thus, a low C value and high N abundance are usually good indicators of this second episode of mixing. With the high luminosity of $\log L_*/L_\odot = 3.1 \pm 0.1$, ET0097 has a high nitrogen abundance, $[\text{N}/\text{Fe}] = 1.18 \pm 0.20$, but also high $[\text{C}/\text{Fe}] = 0.51 \pm 0.10$, so if it has undergone this mixing, it would be inherently more carbon-rich.

During mixing, the most fragile element, Li, is destroyed in the deeper layers of the star, so low Li abundances indicate that mixing has occurred. For main sequence (MS) stars, the Li abundance generally lies along the so-called Spite plateau, $\log \epsilon(\text{Li}) \approx 2.2$. When a star enters the lower RGB phase, the Li at the surface is diluted with material coming from the deeper layers, and the Li abundance sta-

bilizes at an average value of $\log \epsilon(\text{Li}) \approx 1$ along the lower RGB. However, when the second episode of mixing occurs, practically all the remaining Li is destroyed, yielding a very low value of $\log \epsilon(\text{Li}) \leq 0$ (Gratton et al. 2000).

The lithium abundance for ET0097 was obtained by measuring the resonance doublet at 6707 Å, yielding a value of $\log \epsilon(\text{Li}) = -0.12$, but due to the weakness of the line an upper limit of $\log \epsilon(\text{Li}) < 0.17$ was adopted, consistent with most of the Li being destroyed.

Another signature of deep mixing is a low isotope ratio, $\log^{12}\text{C}/^{13}\text{C} < 1.0$ (Spite et al. 2006). To measure $^{12}\text{C}/^{13}\text{C}$, the total carbon abundance was kept constant and the ^{13}C lines were fitted with synthetic spectra with different isotope ratios, see Fig. 4. The ratio was determined to be $\log^{12}\text{C}/^{13}\text{C} = 0.77 \pm 0.03$.

The main signatures of mixing in a high luminosity RGB star are thus present in ET0097, with $\log L_*/L_\odot = 3.1$, $[\text{N}/\text{Fe}] = 1.18$, $\log^{12}\text{C}/^{13}\text{C} = 0.77$ and a best fit of $\log \epsilon(\text{Li}) = -0.12$. We therefore conclude that this star has undergone mixing, and that its carbon abundance was higher at the earlier evolutionary stages.

By assuming most of the nitrogen present in the star was converted from carbon, we get an estimate of the original C abundance at the surface of the star: $[\text{C}/\text{Fe}] \approx 0.8$. In the Galactic halo, mixing in RGB stars is observed to lower the surface C abundance on average by ~ 0.5 (Gratton et al. 2000; Spite et al. 2005), with a scatter of ~ 0.25 dex (Spite et al. 2005, for $-3 \leq [\text{Fe}/\text{H}] \leq -2$), consistent with the correction made here. An online tool to correct for mixing has been provided by Placco et al. (2014), which gives $[\text{C}/\text{Fe}] \approx 0.9$ as the initial abundance for ET0097, while here we adopt the more conservative value of $[\text{C}/\text{Fe}] \approx 0.8$. The estimate for the star’s initial carbon enhancement thus falls under the classical definition of a CEMP ($[\text{C}/\text{Fe}] \geq 0.7$) and the same conclusion is reached using the uncorrected value with the luminosity dependent definition of CEMP stars, from Aoki et al. (2007).

4.4. Alpha elements

The main production sites of the alpha elements (made up of alpha particles) are normal core collapse Type II Supernovae. Early in the star formation history of any galaxy, Type II SN are believed to be the main contributors of metals, so the early ISM holds the imprint of their yields, and stars formed at earlier times typically show an enhancement in $[\alpha/\text{Fe}]$ (e.g., $[\text{Mg}/\text{Fe}] \gtrsim 0.3$). About 1-2 Gyr after the first SN II, Type Ia Supernova start to contribute (e.g., de Boer et al. 2012), and so $[\alpha/\text{Fe}]$ starts to decrease with increasing $[\text{Fe}/\text{H}]$. This so-called ‘knee’, happens around $[\text{Fe}/\text{H}] \sim -1.7$ in Sculptor (Tolstoy et al. 2009).

In ET0097, the abundance measurements for Mg, Ca, and Ti were relatively straight forward, all having many lines that did not show any signs of blending from atomic or molecular lines, see Table 4. On the other hand, all lines for Si were either weak and/or slightly blended. Though the blending was accounted for in the synthetic spectra, it added to the uncertainty of the measurements. However, there were many Si lines available in the observed wavelength range, and the final abundance was measured from the seven best lines. Some of these were weak and unblended, others slightly stronger but were blended. The

number of lines and the reasonable scatter makes the result robust.

There were three S lines in the reddest part of the spectrum ~ 9200 Å, which were affected by reasonably strong CN lines, see the lower panel of Fig. 3. Two S lines were relatively unblended, both of them yielding very similar results (agreeing within 0.05 dex). The line at 9237.5 Å was not used, however, it was consistent with the value obtained for the other two lines.

All alpha elements in ET0097 show an overabundance relative to iron, $[\alpha/\text{Fe}] > 0$, similar to what is seen for other stars in Sculptor and in the Galactic halo at comparable iron abundances, $[\text{Fe}/\text{H}] \approx -2$.

4.5. Odd-Z elements

The abundances of Na, Al, and K were determined from resonance lines that are very sensitive to non-local thermodynamic effects (NLTE) effects. However, similar correction factors are expected for RGB stars with comparable metallicity, T_{eff} and $\log g$, so when comparing abundances of ET0097 with similar stars in the Galactic halo or Sculptor, similar NLTE corrections can be applied. Cayrel et al. (2004) adopted a correction of -0.50 dex for Na in giants, $+0.65$ dex for Al and -0.35 dex for K. Here, the same lines were used for these elements, so similar corrections can be made to the LTE values listed in Table 5. More detailed NLTE calculations for stars with similar stellar parameters are presented in Andrievsky et al. (2007, 2008, 2010).

The Na abundance was determined from the D resonance lines at 5890 Å and 5896 Å, and a weaker line at 8183.3 Å. None of these lines showed any signs of blending and gave the weighted average of $\log \epsilon(\text{Na}) = 3.81 \pm 0.24$.

Two Al lines were visible in the spectrum, the resonance doublet at 3944 Å and 3961.5 Å. Both lines were heavily blended, in particular the line at 3944 Å, so it was not included in the measurement. The result remains rather uncertain, because of the blending and the difficult continuum evaluation in this region, $\log \epsilon(\text{Al}) = 3.62 \pm 0.80$, which is consistent with the line at 3944 Å.

The K abundance was determined from two strong lines at 7665 Å and 7699 Å. Both gave consistent results with a difference of only 0.02 dex. The adopted abundance is therefore $\log \epsilon(\text{K}) = 3.45 \pm 0.07$.

Both Sc and V had many unblended lines available, giving $\log \epsilon(\text{Sc}) = 1.10 \pm 0.04$ and $\log \epsilon(\text{V}) = 2.01 \pm 0.04$.

4.6. Iron-peak elements

In general, Fe-peak elements are believed to be created in supernova explosions. The elements Cr, Mn, Co, and Ni all had many available lines in the observed wavelength range, making it possible to discard those that were blended with molecular lines.

Only one rather weak line was available for Cu, at 5782 Å, in a region of the spectrum that was relatively free of molecular lines. The line barely showed any blending, giving $\log \epsilon(\text{Cu}) = 1.44 \pm 0.26$. Three lines were available for Zn. They only showed minor blending and agree well with each other, $\log \epsilon(\text{Zn}) = 2.68 \pm 0.23$.

4.7. Heavy elements

Abundances for three elements of the lighter n -capture elements were measured: Sr, Y and Zr. Two lines were observed for Sr, one very strong and blended Sr II line at 4078 Å, giving the result $\log \epsilon(\text{Sr})_{4078\text{Å}} = 1.44 \pm 0.34$, and a Sr I line free of blending at 4607 Å, $\log \epsilon(\text{Sr})_{4607\text{Å}} = 1.70 \pm 0.16$. The weighted average of the two yields $[\text{Sr}/\text{Fe}] = 0.71 \pm 0.20$. Yttrium had six lines in the wavelength range, all showing only minor blending and very little scatter, giving the final value $[\text{Y}/\text{Fe}] = 0.34 \pm 0.06$. Five lines are used for the measurement of Zr, three of them slightly blended, giving the result $[\text{Zr}/\text{Fe}] = 0.37 \pm 0.07$. The lighter neutron-capture elements in ET0097 therefore all show overabundance with respect to iron, $[\text{Sr}, \text{Y}, \text{Zr}/\text{Fe}] > 0.3$.

The heavier n -capture elements Ba, La, Ce, and Nd, all had five or more lines available. Of those, La and Ce showed more scatter between lines, $\sigma \sim 0.30$ dex (compared to $\sigma \sim 0.15$ of Ba and Nd), which was to be expected since many of the measured lines for these elements were blended and/or weak. Three Sm lines were measured with a scatter between lines, $\sigma = 0.23$, and the final result is $[\text{Sm}/\text{Fe}] = 0.11 \pm 0.32$. Eu was difficult to measure in this star since the four lines available were all heavily blended. However, all lines agree reasonably well with each other, with a scatter between lines of $\sigma = 0.23$, giving the rather low value $[\text{Eu}/\text{Fe}] = 0.03 \pm 0.42$. No trace of the Eu line at 6645 Å was seen, but an upper limit of $[\text{Eu}/\text{Fe}] < 0.30$ was determined, which is consistent with the four detected lines. The Dy abundance was derived from two weak and blended lines at 3945 Å and 4103 Å, $[\text{Dy}/\text{Fe}] = -0.03 \pm 0.53$. This is consistent with the best fits of two other weak lines at 3984 and 4450 Å. Only upper limits could be determined for those: $[\text{Dy}/\text{Fe}]_{3984\text{Å}} < 0.51$ and $[\text{Dy}/\text{Fe}]_{4450\text{Å}} < 0.23$. There were no detectable lines for the elements Pr, Gd, Tb, Er, and Pb, giving upper limits for these elements in the range $[\text{X}/\text{Fe}] \sim 0.2$ -1.0 dex, which excludes the possibility of extreme overabundances.

With low abundances for both the main s -process elements ($[\text{Ba}/\text{Fe}] < 0$) and main r -process elements ($[\text{Eu}/\text{Fe}] < 0.5$), ET0097 classifies as a CEMP-no star.

5. Error analysis

To evaluate the statistical uncertainties in the abundance determination of a line, $\delta_{\text{noise},i}$, the noise in line-free regions neighboring the line was measured. The error was then determined as when the χ^2 of the fit became larger than that of the noise. Since the spectrum was dominated by molecular lines, line-free regions were not always available. Although the molecular bands were reasonably well fitted as a whole with the synthetic spectra, in some regions individual lines were not. In those cases, the typical deviation of the spectrum from the best synthetic fit was measured and included in the noise estimate.

The individual lines showed different degrees of blending, and for elements with fewer than five measured lines,

this was accounted for by weighting the different measurements with their errors as follows:

$$\log \epsilon(X) = \frac{\sum_{i=1}^{N_X} \log \epsilon(X)_i \cdot w_i}{\sum_{i=1}^{N_X} w_i} \quad (2)$$

The sum runs over N_X lines and the weights of individual lines were defined as:

$$w_i = \frac{1}{\delta_{noise,i}^2} \quad (3)$$

where $\delta_{noise,i}$ is the statistical uncertainty of the abundance measurement of line i . For elements with five or more lines, this was not necessary and normal averages were used to determine the final abundances.

The final error for elements with four or fewer measured lines was calculated as follows:

$$\delta_{noise} = \sqrt{\frac{N_X}{\sum_i w_i}} \quad (4)$$

For elements with five or more lines, the total error from the noise was defined from the scatter of the measurements:

$$\delta_{noise} = \frac{\sigma}{\sqrt{N_X}} \quad (5)$$

Special care was taken in the evaluation of the errors on C and N abundances. These elements were measured over regions of 20 Å and the final value was determined from the average of all measured regions. Measurement errors were calculated using Eq. (5). For C this gave an error of $\delta_C = 0.05$ and $\delta_N = 0.01$ for N.

However, the CH and C₂ lines are sensitive to O values, so the effect of the oxygen error on these abundances was measured and included, yielding a total statistical error of $\delta_{noise,C} = 0.09$.

The CN molecular lines that were used to measure N are sensitive to both C and O abundances. Taking the effect of the uncertainties of these elements on the N measurements into account, the final error is $\delta_{noise,N} = 0.20$.

The systematic errors coming from the uncertainties of the stellar parameters, T_{eff} , $\log g$ and v_t , were measured to be $\Delta[\text{Fe}/\text{H}]_{sp} = 0.10$, and ranging from 0.02 to 0.06 dex for $\Delta[\text{X}/\text{Fe}]_{sp}$ (depending on the element). They were added quadratically to the δ_{noise} to obtain the adopted error,

$$\delta_{total}([\text{X}/\text{Fe}]) = \sqrt{\delta_{noise}(\text{X})^2 + \delta_{noise}(\text{Fe})^2 + \Delta[\text{X}/\text{Fe}]_{sp}^2} \quad (6)$$

6. Results

All element abundances for ET0097 are listed in Table 5.

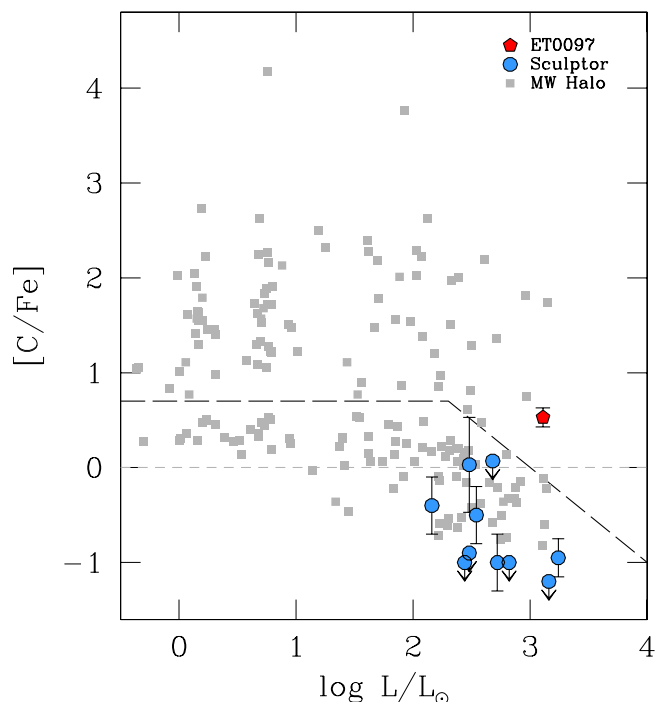


Fig. 5. Carbon in Sculptor and the Galactic halo as a function of luminosity. Dashed line shows the definition of CEMP stars as proposed by Aoki et al. (2007), to account for the mixing in stars at higher luminosities. Halo stars (gray squares) come from Yong et al. (2013), and Sculptor stars (blue circles) from: Tafelmeyer et al. (2010); Frebel et al. (2010); Kirby & Cohen (2012); Starkenburg et al. (2013).

6.1. Carbon in Sculptor

Carbon measurements have been previously attempted only for a limited number of stars in Sculptor, and the available measurements are shown in Fig. 5. The dashed line shows the definition of CEMP stars, as proposed by Aoki et al. (2007), with a slope to account for mixing in RGB stars at higher luminosities, which decreases the carbon abundance and increases the nitrogen at the surface of the star (Gratton et al. 2000; Spite et al. 2006). The high $[\text{N}/\text{Fe}]$, low $\log \epsilon(\text{Li})$, and low $^{12}\text{C}/^{13}\text{C}$ values show that ET0097 has undergone mixing, and was even more carbon-rich in the past, having $[\text{C}/\text{Fe}] \approx 0.8$ (see Section 4.3 for details).

With a measured $[\text{C}/\text{Fe}] = 0.51 \pm 0.10$, ET0097 is the only known star in Sculptor that falls under the definition of a CEMP star, and it seems to be around ~ 1.5 dex higher in carbon than other stars of similar luminosity.

The same stars are shown as a function of iron abundance in Fig. 6b. The most carbon-rich star in the sample, ET0097, is also the most iron-rich, while the fraction of carbon-rich stars increases with decreasing metallicity in the Galactic halo (e.g., Lee et al. 2013 and references therein). Unlike the other Sculptor stars in Fig. 5 and 6b, ET0097 was not chosen for closer observation based on low $[\text{Fe}/\text{H}]$. The UVES spectrum for ET0097 was taken after the C-enhancement was discovered from strong CN molecular lines around 9100-9250 Å. More than 80 other stars were also observed in this wavelength range (Skúladóttir et al. in prep.), and all but the most metal-poor stars have a clear detection of the molecular lines, but only ET0097 stands out, having exceptionally strong CN lines.

To use these CN lines to estimate the C abundances in this sample, some assumptions need to be made about the oxygen and nitrogen. All the stars in this sample are within the central 25' diameter region of Sculptor and bright enough to ensure reasonable signal-to-noise at high spectral resolution. These high luminosity RGB stars ($\log L_*/L_\odot > 2.5$ for all stars, see Table 6) are expected to have undergone similar mixing to ET0097, decreasing the C at the surface and increasing the N abundance. Therefore, a typical value for mixed stars, $[C/N] = -1.2$ (Spite et al. 2005), is adopted here for the sample. Some of the stars already have measured O abundances and show a simple trend with iron, see Fig. 6a. The same trend with $[Fe/H]$ is therefore assumed for stars with unknown O abundances.

The C estimates of 85 stars, calculated with these assumptions, are also shown in Fig. 6b (and listed in Table 6). None of these stars show any sign of being carbon-enhanced, even if corrected for internal mixing, which has been observed to lower the $[C/Fe]$ abundance on the surface of stars by ~ 0.5 dex (Gratton et al. 2000; Spite et al. 2005).

A different approach can be applied. In the sample of Spite et al. (2005), all mixed stars have $[N/Fe] > 0.5$, so by assuming $[N/Fe] = 0$, which is a very conservative lower limit for nitrogen in these stars, we are also able to obtain upper limits for $[C/Fe]$ from the Sculptor CN measurements (assuming the same oxygen values as before), see Table 6. If there are any unmixed stars in our sample, then $[N/Fe] = 0$ is a reasonable abundance estimate for these stars (Spite et al. 2005). Using these assumptions, all 85 stars have $[C/Fe]_{\text{lim}} \leq 0.4$.

So with the exception of ET0097, which clearly stands out from the rest, no other star (mixed or unmixed) in this sample is likely to be inherently carbon-enhanced. In particular, by combining these estimates with the literature data, ET0097 is the only CEMP star from the sample of 22 stars in Sculptor with $[Fe/H] \leq -2$.

6.2. The general abundance pattern

The abundance pattern of ET0097 is compared to what is seen in the Galactic halo and other stars in Sculptor, in Fig. 7. Note that none of the abundances have been corrected for NLTE effects. For many elements this correction can be significant, in particular for Na, Al, and K, reaching up to ~ 0.6 dex. However, the goal here is not to study the trends for these elements. Since both the Galactic halo and Sculptor samples consist of giant stars with similar T_{eff} , $\log g$ and $[Fe/H]$ as ET0097, and have the same measured lines for these elements, any NLTE corrections are expected to be similar for all stars.

ET0097 is the only star in Sculptor in the metallicity range $-2.35 \leq [Fe/H] \leq -1.75$ to have measured carbon and nitrogen, and, in fact, it has the only known nitrogen abundance in this galaxy. To estimate the C and N in stars of similar metallicity, we use the CN molecular lines in the region 9100-9250 Å, from VLT/FLAMES data, see the previous section for details.

Compared to those estimates, ET0097 seems to be enhanced both in C and N with respect to other stars in Sculptor of similar $[Fe/H]$, where the difference in carbon is $\gtrsim 1$ dex, and $\gtrsim 0.5$ dex in nitrogen. Adopting a different $[C/N]$ ratio could increase the N abundance estimate, bringing it closer to ET0097, but that would naturally de-

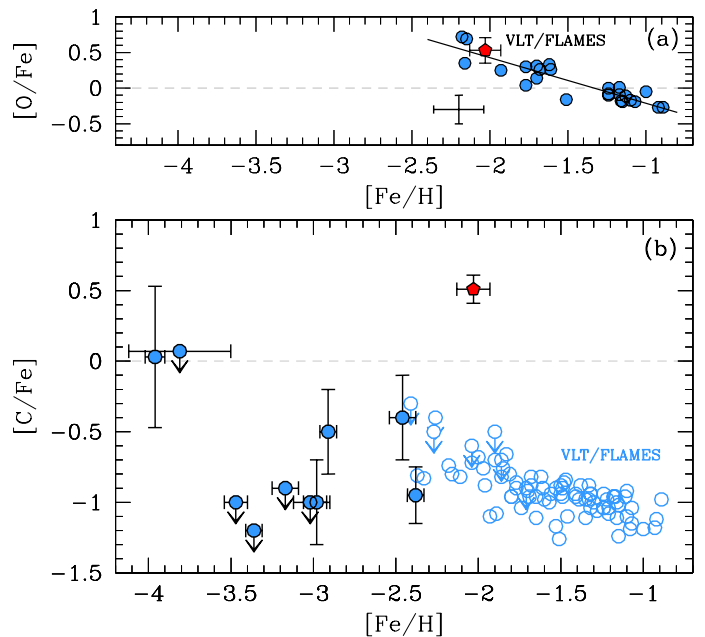


Fig. 6. Same symbols are used as in Fig. 5. (a) Oxygen in Sculptor as a function of $[Fe/H]$. Sculptor stars (blue filled circles) come from Hill et al. in prep. Representative error bar for the measurements is shown; (b) Carbon in Sculptor as a function of $[Fe/H]$. Solid points are direct carbon measurements of the stars shown in Fig. 5. Open circles show estimates of C abundances for 85 stars (VLT/FLAMES spectra) from CN molecular lines in the wavelength range 9100-9250 Å. Ratio typical for mixed stars, $[C/N] = -1.2$ (Spite et al. 2005), is assumed, and for stars with unknown oxygen abundance, a simple trend of $[O/Fe]$ with $[Fe/H]$ is adopted, as shown with a line in (a). Two stars from Starkenburg et al. 2013 that have the same $[C/Fe]$ at $[Fe/H] \sim -3$ are moved by 0.02 dex to each side, to be visible as two stars. Same is done for two stars with similar C estimates at $[Fe/H] = -2.35$.

crease the C, making the difference there even bigger. Comparing ET0097 to carbon-normal, mixed RGB stars in the Galactic halo (Spite et al. 2005), the nitrogen seems to be rather high, but it does not stand out significantly from the scatter. The C in this star is however clearly enhanced compared to similar stars in the Galactic halo. Finally, we note that the $[C+N/Fe]$ in the Sculptor sample seems to be lower than what is observed in the Galactic halo.

In Fig. 7, it is clear that when other elements up to Zn are compared with the mean for Sculptor and the Galactic halo, ET0097 does not stand out significantly in any way, and falls within the scatter of stars with similar metallicity. However, ET0097 does show a different pattern in elements heavier than Zn. The lighter neutron-capture elements (sometimes called weak r -process elements), Sr, Y, and Zr, are enhanced compared to what is typical in Sculptor, while the heavier n -capture elements are depleted, or at the lower end of the trend (Ba). The Galactic halo shows a very large scatter of the n -capture elements in the metallicity range $-3.0 \leq [Fe/H] \leq -2.0$, so both ET0097 and other stars in Sculptor fall within the scatter seen in these elements, with the exception of Sr and Y, which appear above the observed scatter.

Since ET0097 shows high abundances of light n -capture elements and low abundances of the heavier n -capture elements, naturally the abundance ratios $[Sr, Y, Zr/Ba]$ are

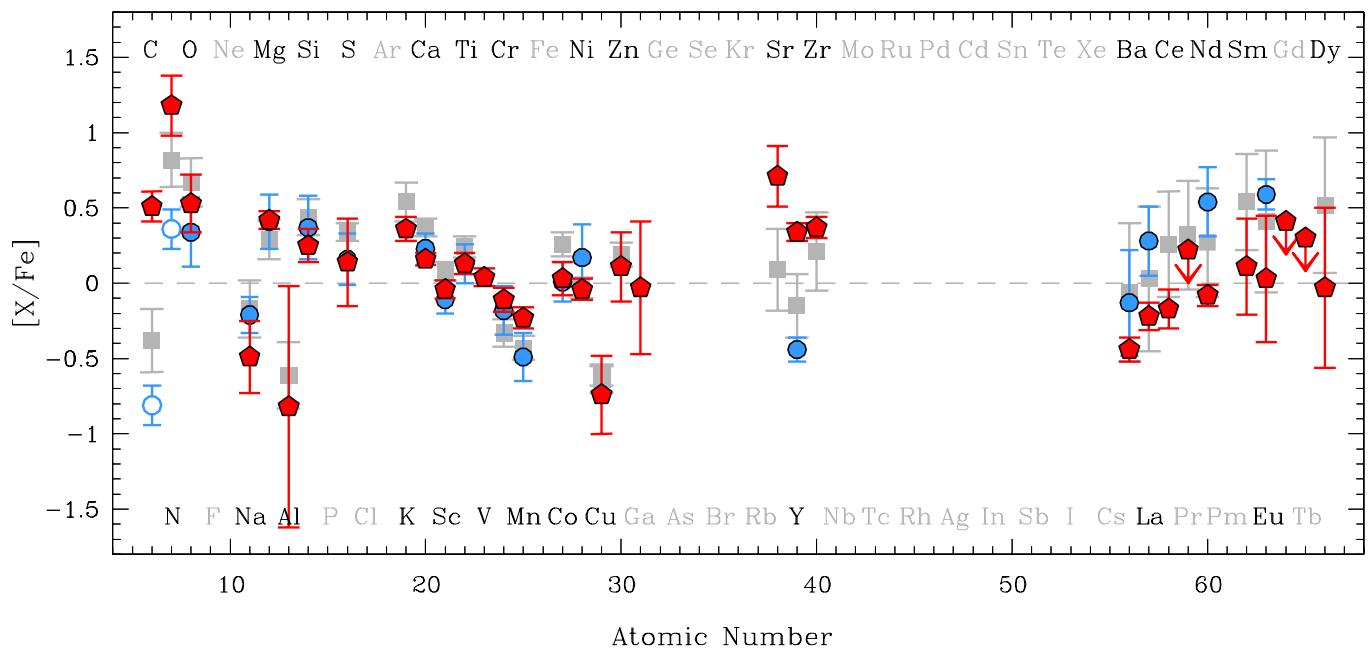


Fig. 7. Element abundances for ET0097 (red pentagons), Sculptor (blue circles) and the Galactic halo (gray squares). Sculptor abundances are averaged over all stars with $-2.35 \leq [\text{Fe}/\text{H}] \leq -1.75$. For Sculptor, most elements come from Hill et al. in prep. Exceptions are C and N estimated here from CN molecular lines (see Fig. 6 for detail), and S which comes from Skúladóttir et al. in prep. The Galactic halo abundances are averaged over stars with $-3.0 \leq [\text{Fe}/\text{H}] \leq -2.0$. Abundance averages for C and N in the Galactic halo are taken from mixed, C-normal stars in Spite et al. (2005). Other elements up to Zn are taken from Cayrel et al. (2004), with the exceptions of S, which is from Spite et al. (2011), and Cu, which is taken from both halo and disk stars in Mishenina et al. (2002). Elements heavier than Zn come from François et al. (2007). Error bars for Sculptor and the Galactic halo represent 1σ of the scatter of $[\text{X}/\text{Fe}]$ over each sample. No NLTE corrections have been applied, but are expected to be similar for all stars.

high, see Fig. 8. Here ET0097 is clearly different from the trend seen in the Galactic halo and in Sculptor. Similar abundance ratios are certainly seen in the halo (e.g., Honda et al. 2004; François et al. 2007), but typically at lower iron abundance ($[\text{Fe}/\text{H}] \lesssim -3$). This result is not limited to a comparison with Ba, ET0097 still stands out when any of the other heavier n -capture elements are used as a reference element. In fact, ET0097 shows the same relation to the heavier n -capture elements as seen in the Galactic halo, see Fig. 9.

7. Origin of the abundance pattern

7.1. Alpha and iron-peak elements

In ET0097, alpha and Fe-peak elements from O to Zn show abundances comparable to what is seen both in the Galactic halo and in Sculptor for stars with similar $[\text{Fe}/\text{H}]$, (see Fig. 7). The most probable explanation is that the bulk of these elements comes from similar sources, such as low-metallicity Type II supernovae of 11-40 M_{\odot} (Woosley & Weaver 1995), which are believed to be the main producers of these elements in the early universe, or possibly massive zero-metallicity SN of 10-100 M_{\odot} (Heger & Woosley 2010), which have been shown to predict similar abundances as seen in the Galactic halo, hence comparable with ET0097.

7.2. Carbon-enhancement

The origin of the carbon enhancement in CEMP-no stars is still debated and a variety of processes have been invoked (see, e.g., Norris et al. 2013).

In some of these scenarios, the carbon enhancement is explained by mass transfer from a companion. Three different HR velocity measurements for ET0097 were obtained in Hill et al. (in prep.), Skúladóttir et al. (in prep.), and this work. A comparison was made between the two other studies for the 86 stars they had in common. ET0097 showed similar scatter in its velocity measurements compared to other stars in Sculptor. On average the difference between the samples was 1.5 km/s, and ET0097 had a difference of 1.4 km/s in the two measurements. Therefore, close binarity that favors mass transfer seems unlikely, though it cannot be completely excluded with the present data.

However, even if this star does have a companion or did at some point, the abundance pattern is not easily explained with binarity. Mass transfer from an AGB-companion as seen in CEMP- s stars can be excluded because $[\text{Y}/\text{Ba}] < 0$ is expected (Travaglio et al. 2004), which is clearly not consistent with ET0097 (see Fig. 8). Mass transfer from rapidly rotating stars, which are known to produce a lot of C, is also a possible source for the carbon enhancement. But from these stars strong enhancements in N and O, comparable to the C enhancement, are also expected (Meynet et al. 2006), and this is not consistent with the observations, which in particular show no enhancement in oxygen compared to other Sculptor and halo stars. This scenario can therefore be excluded.

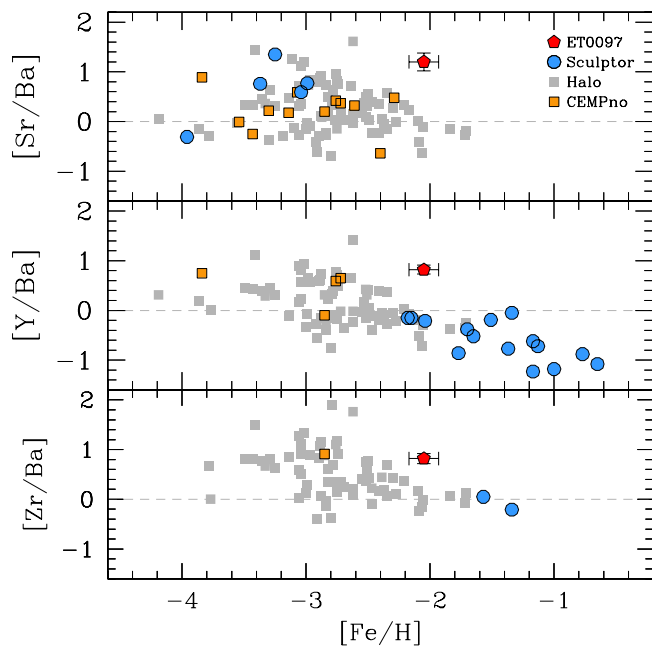


Fig. 8. Light neutron-capture elements, Sr, Y, Zr, with respect to Ba, as a function of Fe abundance. Sculptor stars are from Hill et al. in prep.; Shetrone et al. (2003); Geisler et al. (2005); Tafelmeyer et al. (2010); Starkenburg et al. (2013). Galactic halo stars are taken from: Johnson & Bolte (2002); Honda et al. (2004); Aoki et al. (2005); François et al. (2007). CEMP-no stars in the halo are taken from a compilation by Allen et al. (2012), including data from: Norris et al. (2001, 2002); Giridhar et al. (2001); Preston & Sneden (2001); Aoki et al. (2002a,b,c, 2004, 2007); Depagne et al. (2002); Honda et al. (2004); Barklem et al. (2005); Cohen et al. (2006, 2008); Sivarani et al. (2006).

Another possible scenario is that CEMP-no stars formed out of gas that has been enriched by faint supernovae with mixing and fallback which produce significant amounts of C but minimal Fe. Apart from the excess of carbon, faint SN show a general abundance pattern that is very different from normal Type II SN, with an excess of N and O. The ejecta from these stars are also predicted to have a very pronounced odd-even effect among iron-peak elements, showing up as very low abundance ratios, e.g., $[V/Fe]$ and $[Mn/Fe]$, which are not compatible with the results presented here.

However, by assuming ET0097 formed out of gas containing a mixture of yields from faint SN and normal SN, it is possible to explain the carbon enhancement in this star. By assuming that normal SN Type II enrich the gas up to $[Fe/H] \approx -2$, and that the gas was already pre-enriched with faint SN yields, as presented by Iwamoto et al. (2005) to match the hyper metal-poor star HE0107-5240, we require that the fraction of faint SN to normal SN is such that the gas reaches $[C/Fe] = 0.8$ (a reasonable assumption for the initial value for ET0097). Though these faint SN yields also show enhancements in N and O, they are considerably smaller than for C. Therefore, the addition of these elements in ET0097 from faint SN would be undetectable in this mixture of yields, falling well within the error of the measurements. The effects on the abundances of other elements in the star are even less pronounced. All the peculiarities of the faint SN yields are swamped by the SN Type II enrichment, leaving the high $[C/Fe]$ value as

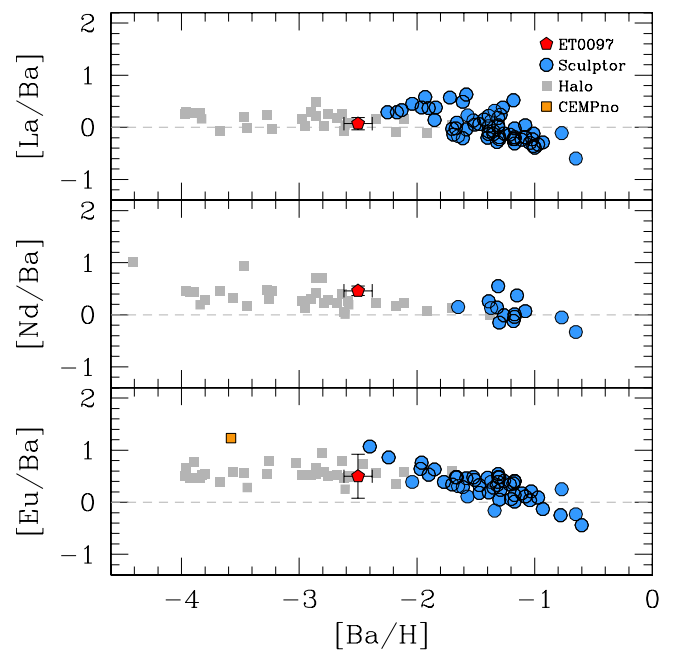


Fig. 9. The relative abundances of the heavier neutron-capture elements. References are the same as in Fig. 8.

the only evidence of its contribution. Therefore, it is indeed possible that the carbon enhancement in ET0097 is the result of (partial) enrichment with the products of faint SN. This is discussed in more detail in Section 8.

7.3. The lighter *n*-capture elements

The main *r*- and *s*-process are excluded as dominant sources of Sr, Y, and Zr in ET0097 because they are predicted to produce much higher abundance ratios of heavy to light neutron-capture elements than are consistent with the data. The enhancements of Sr, Y, and Zr, most probably come from the weak *r*-process (e.g., Arcones & Montes 2011), which is predicted to produce significant amount of these elements, but minimal heavier *n*-capture elements ($Z \geq 56$). Another possibility for the source of these elements is the weak *s*-process that occurs in fast-rotating massive zero-metallicity stars. Models of these stars have been able to reproduce the scatter of these elements observed in the Galactic halo (Cescutti & Chiappini 2014). However, the data presented here are not sufficient to distinguish between the different possible scenarios, and models that predict excesses of Sr, Y, and Zr, without significant effects on other element abundances, are consistent with observations of ET0097.

In the Galactic halo, a few stars showing strong signatures of the weak *r*-process (or weak *s*-process) have been found and studied in detail. Two of those stars, HD 88609 ($[Fe/H] = -3.07$) and HD 122563 ($[Fe/H] = -2.77$) from Honda et al. (2007) are compared to ET0097 in Fig. 10. To ensure a useful comparison of the abundance pattern of the *n*-capture elements in these stars, they have all been normalized to the $[Y/H]$ value of HD 88609. The absolute values of $[X/H]$ for the *n*-capture elements are much higher in ET0097 than in the other, more metal-poor stars. In fact, when comparing to Fe, ET0097 is more enriched in Sr, Y, and Zr than the other two stars ($[Y/Fe]_{ET0097} = 0.35$, $[Y/Fe]_{HD\ 88609} = -0.12$ and $[Y/Fe]_{HD\ 122563} = -0.37$).

Also included in Fig. 10 (with the same normalization) is the n -capture rich star CS 22892-052 from Sneden et al. (2003), which is believed to show a pure signature of the main r -process.

The relative abundance pattern in the n -capture elements of ET0097 is comparable to the two Honda stars (see Fig. 10), making it very likely that these stars were polluted by similar processes. The only exception is Pr, which seems to be much lower in ET0097 than in the others.¹ Apart from this one element, the abundance patterns of the three stars are comparable. The main r -process rich star, CS 22892-052, shows a completely different pattern, and so it is clear that the origin of its n -capture elements is different from the other stars. ET0097 and the two Honda stars show similar signatures of the weak r -process, possibly with some contamination from the main r -process.

Finally, it should be noted that the weak s -process in fast-rotating, zero-metallicity massive stars has been proposed to simultaneously enrich gas with C, N O and the lighter neutron-capture elements (Chiappini et al. 2006; Frischknecht et al. 2012; Cescutti & Chiappini 2014). However, these models predict an enhancement of O comparable with the C enhancement, which is not observed in ET0097. It should also be noted that neither of the Honda stars are enhanced in carbon, $[C/Fe] \lesssim -0.40$ for both stars (Honda et al. 2004), which is consistent with the idea that the enhancements of carbon and the light n -capture elements come from two different processes. This is also supported by the top panel of Fig. 8, where the CEMP-no stars do not show any obvious trend of $[Sr/Ba]$ with $[Fe/H]$, different from the normal population, and the same is true for $[Sr/Fe]$ with $[Fe/H]$ (See, e.g., Cescutti & Chiappini 2014, their Fig. 1).

8. Possible formation scenario

To explain the abundance pattern seen in ET0097, the formation scenario must include a plausible explanation for carbon and lighter neutron-capture enhancements at such high $[Fe/H] = -2.03 \pm 0.10$. Usually these are seen at lower values, $[Fe/H] \lesssim -3$, in the Galactic halo. The star ET0097 is also depleted in the heavier n -capture elements compared to other stars of similar iron abundance in Sculptor, see Fig. 7.

These peculiarities of ET0097 therefore seem to indicate that it was not formed from the same material as most other stars observed in Sculptor. One possible scenario is that this star was formed in one of the progenitor (mini)-halos of Sculptor that formed at high-redshift and initially evolved independently (e.g., Salvadori & Ferrara 2009), also sometimes called inhomogeneous mixing.

Although the C-enhancement in CEMP-no stars is usually associated with faint SNe, which have relatively high C yields compared to their Fe-peak elements production (e.g., Iwamoto et al. 2005), pollution by faint SNe alone cannot enrich a gas cloud up to a metallicity of $[Fe/H] \approx -2$ (Salvadori & Ferrara 2012; Cooke & Madau 2014), and the

¹ The Pr lines at 4179.4 and 4189.5 Å, used by Honda et al. (2007), are severely blended with CH molecular lines in ET0097, and therefore cannot be used for the abundance determination, but are consistent with no lines being observed. Instead the upper limit for Pr was determined from lines at 4408.8 and 4496.5 Å, both giving similar results.

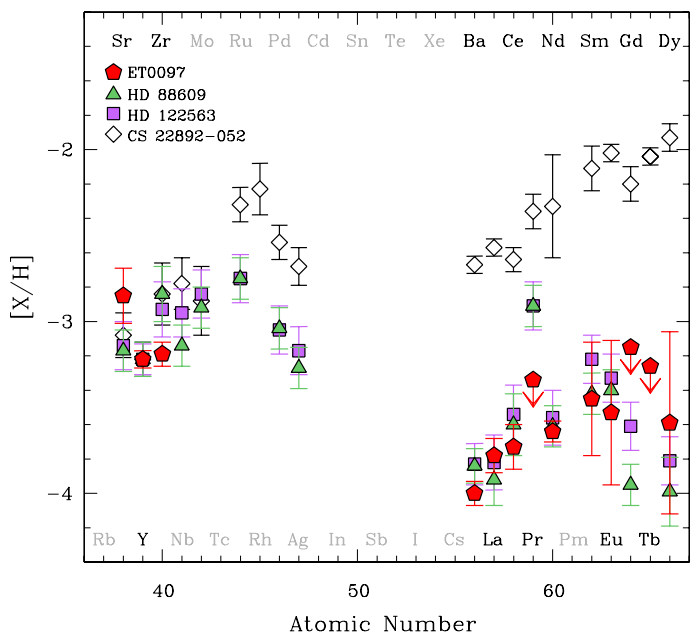


Fig. 10. The n -capture elements of ET0097 compared to two stars with weak r -process enhancements, HD 88609 and HD 122563 (Honda et al. 2007), and one main r -process rich star, CS 22892-052 (Sneden et al. 2003). All four stars are normalized to the same $[Y/H]$ value as HD 88609.

general abundance pattern of the yields of such stars is very different from ET0097. However, as discussed in the previous section, it is possible that ET0097 was formed out of material that contained a mixture of yields from faint SNe and normal core collapse SNe.

It has been shown that massive zero-metallicity SN are able to pollute small self-enriched systems up to high $[Fe/H] \approx -2$ (Salvadori et al. 2007; Karlsson et al. 2008). So one possibility is that ET0097 was formed in a mini-halo that had only been enriched by the first generation of stars, a population containing both zero-metallicity core collapse SN and faint SN. If that is the case, we should be able to estimate the required relative contributions of faint and "normal" primordial supernovae to simultaneously account for the observed C and Fe abundances and the lighter n -capture elements.

To test this idea, we assume a very simple scenario where this primordial population forms in a single burst of mass M_* , with a Salpeter IMF in the mass range 10-100 M_\odot . A fraction F_F of the star-forming gas goes into faint SN (as described by Iwamoto et al. 2005 for HE0107-5240), and a fraction $F_N = 1 - F_F$ goes into normal zero-metallicity SN, (as described by Heger & Woosley 2010 with standard mixing and energy $E_{SN} = 1.2 \cdot 10^{51}$ erg)².

The iron abundance of a gas cloud with mass M_g , and a mass of iron M_{Fe} can be approximated by:

$$[Fe/H] = \log \left(\frac{M_{Fe}}{M_g} \right) - \log \left(\frac{M_{Fe}}{M_H} \right)_\odot \quad (7)$$

² In the normal SN case, the yields for carbon are taken from Table 8 in Heger & Woosley (2010), and the iron taken from ⁵⁶Ni yields in their Table 6 for the same mass values. Both elements are integrated in the same way over a Salpeter IMF.

Similarly, we get an expression for the mass of carbon in the gas, M_C ,

$$[\text{C}/\text{Fe}] = \log\left(\frac{M_C}{M_{\text{Fe}}}\right) - \log\left(\frac{M_C}{M_{\text{Fe}}}\right)_{\odot} \quad (8)$$

By assuming solar abundances from Grevesse & Sauval (1998) the mass of Fe and C needed to enrich the gas up to $[\text{Fe}/\text{H}] = -2.03$ and $[\text{C}/\text{Fe}] = 0.8$ is

$$M_{\text{Fe}} = 10^{-4.78} \cdot M_g \quad (9)$$

$$M_C = 14.2 \cdot M_{\text{Fe}} \quad (10)$$

The total amount of iron and carbon produced in a star forming episode of total mass M_* , is therefore

$$M_{\text{Fe}} = \mathcal{Y}_N(\text{Fe})F_N M_* + \mathcal{Y}_F(\text{Fe})F_F M_* \quad (11)$$

$$M_C = \mathcal{Y}_N(\text{C})F_N M_* + \mathcal{Y}_F(\text{C})F_F M_* \quad (12)$$

where the yields \mathcal{Y} of Fe and C, are the masses of these elements (in M_{\odot}) that are produced and released into the environment by each M_{\odot} of gas transformed into stars. The Fe yields in faint SNe are negligible, $\mathcal{Y}_F(\text{Fe}) \ll \mathcal{Y}_N(\text{Fe}) = 2.0 \cdot 10^{-3}$, and the carbon yields of the faint and normal SNe are respectively: $\mathcal{Y}_F(\text{C}) = 4.2 \cdot 10^{-3}$ (Iwamoto et al. 2005), and $\mathcal{Y}_N(\text{C}) = 1.0 \cdot 10^{-2}$ (Heger & Woosley 2010). Thus Eq. (9)-(12) give $F_N = 0.19$ and $F_F = 0.81$.

By defining the star formation efficiency, f_* , as the fraction of gas turned into stars, the total mass of the primordial population is

$$M_* = f_* M_g \quad (13)$$

Combining this with Eq. (9) and (11), gives $f_* = 0.044$. This is an upper limit, since more realistic calculations should take into account that stars with different masses do not explode all at once and some of the gas is ejected by SNe of massive stars before the lower mass stars start to contribute, leaving less gas to enrich.

This scenario is also able to explain the overabundance of the lighter n -capture elements (Sr, Y, Zr), seen in ET0097, if certain requirements are fulfilled. Arcones & Montes (2011) describe the weak r -process in neutrino-driven winds from core collapse supernovae of progenitor mass $10 M_{\odot} \leq M \leq 25 M_{\odot}$. Using their yields and going through similar calculations to those above, the weak process has to occur in $\sim 10\%$ of the total stellar mass formed as a normal SN in the mass range 10 - $25 M_{\odot}$, to account for the Sr, Y, and Zr abundances observed in ET0097.

Heger & Woosley (2010) have shown that their yields are consistent with the general abundance pattern seen in low-metallicity halo stars (such as in Cayrel et al. 2004) for other elements up to Zn, and it is therefore reasonable to conclude that they are also consistent with ET0097.

With this very simple calculation, we show that ET0097 is compatible with having been enriched with the first stellar generation. We are able to explain both the high iron abundance, and the overabundances of carbon and the lighter n -capture elements.

Another (similar) possibility is that this star was formed in a (mini)-halo, where the first stellar generation was dominated by faint SN, and then normal (nonzero-metallicity) Type II SNe (Woosley & Weaver 1995), which have comparable C and Fe yields to the zero-metallicity case, enriched the gas up to $[\text{Fe}/\text{H}] \approx -2$.

In both of these scenarios, it is necessary that the (mini)-halo is large enough to retain some of its gas for the next generation(s) of stars, and that the stellar population of zero-metallicity stars is dominated by faint SN. This is consistent with de Bressana et al. (2014) who show that a stellar population of zero-metallicity stars dominated by faint SN is able to produce the CEMP fraction observed in the halo.

9. The CEMP-no fraction in Sculptor

In total, 22 stars in Sculptor with $[\text{Fe}/\text{H}] \leq -2$ have C measurements or upper limits (Frebel et al. 2010; Tafelmeyer et al. 2010; Kirby & Cohen 2012; Starkenburg et al. 2013; and this work). Only one of them falls into the category of a CEMP-no star, making the fraction $4.5_{-3.8}^{+10.5}\%$ (errors are derived using Gehrels 1986).

In the Galactic halo, the proportion of CEMP-no stars (when the RGB stars have been corrected for internal mixing and CEMP- s and CEMP- s/r stars have been excluded from the sample) is $20 \pm 2\%$ (compilation of data and correction for mixing comes from Placco et al. 2014³, with Poisson errors derived from Gehrels 1986). If this fraction was the same in Sculptor, $p = 0.20$, then from a sample of $N = 22$ stars, the expected number of CEMP-no stars with $[\text{C}/\text{Fe}] \geq 0.7$ is $R_{exp} = Np \pm \sqrt{N(1-p)p} = 4.4 \pm 1.9$. However, only one is found. In the lower metallicity range, $[\text{Fe}/\text{H}] \leq -3$, the fraction of CEMP stars in the Galactic halo is $p = 0.43_{-0.05}^{+0.06}$ (Placco et al. 2014). In Sculptor, $N = 8$ stars in this range have measured carbon or upper limits, so the expected number of stars with $[\text{C}/\text{Fe}] \geq 0.7$ (once they have been corrected for mixing), is $R_{exp} = 3.4 \pm 1.4$, but none are found. The fraction of CEMP-no stars in the currently observed Sculptor sample is thus lower than in the Galactic halo, and the difference is statistically significant.

This ratio can be affected by the fact that no stars with $[\text{Fe}/\text{H}] \leq -4.0$ have been found so far in Sculptor, while those stars predominantly fall into the CEMP-no category in the halo. Looking at the range $-2.5 \leq [\text{Fe}/\text{H}] \leq -2$, the fraction of CEMP-no stars in Sculptor is $8_{-7}^{+19}\%$, which is consistent with that found in the halo, $5_{-2}^{+3}\%$ (data coming from Placco et al. 2014, with Poisson errors derived from Gehrels 1986). The expected number of CEMP-no stars in this range, should the Sculptor fraction be the same as in the halo, is $R_{exp} = 0.6_{-0.6}^{+0.8}$ stars, which is consistent with the one star found. Only one observed (C-normal) star in Sculptor falls in the range $-3 < [\text{Fe}/\text{H}] < -2.5$, so little can be said about the CEMP-no fraction there. However, for the lowest metallicity range, $-4 \leq [\text{Fe}/\text{H}] \leq -3$, no CEMP-no star is found in Sculptor out of a sample of eight stars, giving the Poisson upper limit of the fraction, 23% . In the same metallicity range in the halo, the fraction is $39_{-5}^{+6}\%$. The expected number of CEMP-no stars in the Sculptor sample, should the fraction be the same as in the halo is $R_{exp} = 3.1 \pm 1.4$ stars, while none are found. Although still poorly constrained due to low number statistics, the CEMP-no fraction in Sculptor is therefore consistent with

³ The Placco et al. (2014) sample is based on the most recent version of the SAGA database (Suda et al. 2008) and the compilation of literature data by Frebel et al. (2010) and data published since then. For individual references see Placco et al. (2014).

the Galactic halo at higher metallicities ($-2.5 \leq [\text{Fe}/\text{H}] \leq -2$), while it appears to be different at the lowest metallicity end, $-4 \leq [\text{Fe}/\text{H}] \leq -3$ (see also: Starkenburg et al. 2013).

It remains puzzling that no CEMP-no stars are found at lower metallicities in Sculptor, while ET0097 has a rather high metallicity for such objects, $[\text{Fe}/\text{H}] = -2.03 \pm 0.10$. If the CEMP-no stars indeed show imprints of the very first stars, they would be expected to be more common at the lowest metallicities, also in dwarf spheroidal galaxies such as Sculptor. This apparent discrepancy is not easily explained, and it cannot be excluded that CEMP-no stars are a mixed population with different formation scenarios (an overview is given in Norris et al. 2013). However, we want to emphasize that the CEMP-no fraction in Sculptor is still very poorly constrained, with an upper limit of $\sim 25\%$ both at the high and the low-metallicity end, and not very constraining lower limits ($< 2\%$). Although the CEMP-no fraction at the low-metallicity end in Sculptor seems to be different from the halo, a similar trend is still possible where the fraction increases with lower $[\text{Fe}/\text{H}]$, and should be expected. The effect of the environment on the CEMP-no fraction is still not well understood, and will be explored in greater detail in Salvadori et al. in prep.

10. Conclusions

After unusually strong CN molecular lines were discovered in the star ET0097, a follow-up spectrum at high-resolution and over a long wavelength range was taken with the ESO/VLT/UVES spectrograph. Detailed abundance analysis shows that with $[\text{C}/\text{Fe}] = 0.51 \pm 0.10$, ET0097 is the most carbon-rich VMP star known in Sculptor. Having a luminosity of $\log L_*/L_\odot = 3.1$, this star is expected to have undergone mixing, lowering the carbon at the surface of the star and increasing the nitrogen. This is confirmed by the high N of the star, $[\text{N}/\text{Fe}] = 1.18 \pm 0.20$, the low isotope ratio $\log^{12}\text{C}/^{13}\text{C} = 0.77 \pm 0.03$, and the low Li abundance $\log \epsilon(\text{Li}) < 0.17$. The original C abundance of ET0097 is therefore estimated to be $[\text{C}/\text{Fe}] \approx 0.8$, making this the only known CEMP in Sculptor.

The star shows normal abundances for all alpha and Fe-peak elements from O to Zn, consistent with what is seen both in the Galactic halo and Sculptor for giants of similar metallicities. Compared to other stars in Sculptor, ET0097 is enhanced in the lighter n -capture elements (Sr, Y, Zr), and shows low abundances of the heavier n -capture elements, making this a CEMP-no star. The abundance ratios $[\text{Sr}, \text{Y}, \text{Zr}/\text{Ba}]$ are high, especially in relation to the Fe abundance of the star. The abundance pattern of the n -capture elements is comparable to what is seen in stars that are believed to have been polluted by the weak r -process.

One possible scenario to explain the peculiar abundance pattern of ET0097 is that the star formed in one of the low-mass progenitor halos of Sculptor, which had only been enriched by a primordial population consisting of a mixture of faint SN ($\sim 80\%$) and zero-metallicity core collapse SN ($\sim 20\%$). Another possibility is that this star was formed in a halo where the first stellar generation consisted of faint SN only, and then normal Type II SNe polluted the gas up to $[\text{Fe}/\text{H}] \approx -2$.

In addition to the abundance analysis for ET0097, ESO/VLT/FLAMES data in the wavelength range 9100–9250 Å was used to determine estimates and upper lim-

its for carbon in 85 Sculptor stars, including 11 stars with $[\text{Fe}/\text{H}] \leq -2$. No other star in the sample was found to be carbon-enhanced.

In the Galactic halo, Placco et al. (2014) have carefully determined the fraction of CEMP stars in a sample of ~ 500 stars with $[\text{Fe}/\text{H}] \leq -2$. The RGB stars in their sample have been corrected for internal mixing, and CEMP- s and CEMP- s/r stars have been excluded. Using these very detailed results, we are able to compare the CEMP-no fraction observed in Sculptor to that seen in the halo. The fraction of CEMP-no to C-normal stars in the entire sample of observed Sculptor stars with $[\text{Fe}/\text{H}] \leq -2$, is $4.5^{+10.5}_{-3.8}\%$. This is lower than that seen in the Galactic halo, $20 \pm 2\%$ (Placco et al. 2014), and the difference is statistically significant.

If we explore this further in different metallicity bins, then for $-2.5 \leq [\text{Fe}/\text{H}] \leq -2$, the observed CEMP-no fraction in Sculptor is $8^{+19}_{-7}\%$, consistent with that found in the halo, $5^{+3}_{-2}\%$. At the lowest metallicity end in Sculptor, $-4 \leq [\text{Fe}/\text{H}] \leq -3$, the CEMP-no fraction is $0^{+23}\%$, which is statistically significantly lower than that observed in the Galactic halo, $39^{+6}_{-5}\%$. The carbon measurements in Sculptor are still few, so the CEMP-no fraction is poorly constrained, but, at least at the lowest metallicity end, the CEMP-no fraction in Sculptor seems to be fundamentally different from what is seen in the Galactic halo.

Acknowledgements. We thank ESO for granting us Directors Discretionary time to allow us to rapidly follow up this very interesting star. The authors are indebted to the International Space Science Institute (ISSI), Bern, Switzerland, for supporting and funding the international team "First stars in dwarf galaxies". A. S. thanks Anna Frebel for useful advice and insightful suggestions. S. S. acknowledges support from the Netherlands Organisation for Scientific Research (NWO), VENI grant 639.041.233. E. S. gratefully acknowledges the Canadian Institute for Advanced Research (CIFAR) Global Scholar Academy.

References

- Allen, D. M., Ryan, S. G., Rossi, S., Beers, T. C., & Tsangaris, S. A. 2012, *A&A*, 548, A34
- Alonso, A., Arribas, S., & Martínez-Roger, C. 1999, *A&AS*, 140, 261
- Alvarez, R. & Plez, B. 1998, *A&A*, 330, 1109
- Andrievsky, S. M., Spite, M., Korotin, S. A., et al. 2010, *A&A*, 509, A88
- Andrievsky, S. M., Spite, M., Korotin, S. A., et al. 2007, *A&A*, 464, 1081
- Andrievsky, S. M., Spite, M., Korotin, S. A., et al. 2008, *A&A*, 481, 481
- Aoki, W., Beers, T. C., Christlieb, N., et al. 2007, *ApJ*, 655, 492
- Aoki, W., Honda, S., Beers, T. C., et al. 2005, *ApJ*, 632, 611
- Aoki, W., Norris, J. E., Ryan, S. G., Beers, T. C., & Ando, H. 2002a, *ApJ*, 576, L141
- Aoki, W., Norris, J. E., Ryan, S. G., Beers, T. C., & Ando, H. 2002b, *PASJ*, 54, 933
- Aoki, W., Norris, J. E., Ryan, S. G., Beers, T. C., & Ando, H. 2002c, *ApJ*, 567, 1166
- Aoki, W., Norris, J. E., Ryan, S. G., et al. 2004, *ApJ*, 608, 971
- Arcones, A. & Montes, F. 2011, *ApJ*, 731, 5
- Azzopardi, M., Lequeux, J., & Westerlund, B. E. 1986, *A&A*, 161, 232
- Barklem, P. S., Christlieb, N., Beers, T. C., et al. 2005, *A&A*, 439, 129
- Battaglia, G., Helmi, A., Tolstoy, E., et al. 2008, *ApJ*, 681, L13
- Biémont, E., Palermi, P., & Quinet, P. 1999, *Ap&SS*, 269, 635
- Brooke, J. S. A., Ram, R. S., Western, C. M., et al. 2014, *ApJS*, 210, 23
- Cayrel, R., Depagne, E., Spite, M., et al. 2004, *A&A*, 416, 1117
- Cescutti, G. & Chiappini, C. 2014, *A&A*, 565, A51
- Chiappini, C., Hirschi, R., Meynet, G., et al. 2006, *A&A*, 449, L27

- Cohen, J. G., Christlieb, N., McWilliam, A., et al. 2008, *ApJ*, 672, 320
- Cohen, J. G., McWilliam, A., Shtetman, S., et al. 2006, *AJ*, 132, 137
- Cooke, R. J. & Madau, P. 2014, *ApJ*, 791, 116
- de Bannassuti, M., Schneider, R., Valiante, R., & Salvadori, S. 2014, *ArXiv e-prints*
- de Boer, T. J. L., Tolstoy, E., Hill, V., et al. 2012, *A&A*, 539, A103
- de Boer, T. J. L., Tolstoy, E., Saha, A., et al. 2011, *A&A*, 528, A119+
- Dekker, H., D'Odorico, S., Kaufer, A., Delabre, B., & Kotzlowski, H. 2000, in *Society of Photo-Optical Instrumentation Engineers (SPIE) Conference Series*, Vol. 4008, *Optical and IR Telescope Instrumentation and Detectors*, ed. M. Iye & A. F. Moorwood, 534–545
- Depagne, E., Hill, V., Spite, M., et al. 2002, *A&A*, 390, 187
- François, P., Depagne, E., Hill, V., et al. 2007, *A&A*, 476, 935
- Frebel, A., Kirby, E. N., & Simon, J. D. 2010, *Nature*, 464, 72
- Freudling, W., Romaniello, M., Bramich, D. M., et al. 2013, *A&A*, 559, A96
- Frischknecht, U., Hirschi, R., & Thielemann, F.-K. 2012, *A&A*, 538, L2
- Gehrels, N. 1986, *ApJ*, 303, 336
- Geisler, D., Smith, V. V., Wallerstein, G., Gonzalez, G., & Charbonnel, C. 2005, *AJ*, 129, 1428
- Giridhar, S., Lambert, D. L., Gonzalez, G., & Pandey, G. 2001, *PASP*, 113, 519
- Gratton, R. G., Sneden, C., Carretta, E., & Bragaglia, A. 2000, *A&A*, 354, 169
- Grevesse, N. & Sauval, A. J. 1998, *Space Science Reviews*, 85, 161
- Groenewegen, M. A. T., Lançon, A., & Marescaux, M. 2009, *A&A*, 504, 1031
- Gustafsson, B., Edvardsson, B., Eriksson, K., et al. 2008, *A&A*, 486, 951
- Heger, A. & Woosley, S. E. 2010, *ApJ*, 724, 341
- Honda, S., Aoki, W., Arimoto, N., & Sadakane, K. 2011, *PASJ*, 63, 523
- Honda, S., Aoki, W., Ishimaru, Y., & Wanajo, S. 2007, *ApJ*, 666, 1189
- Honda, S., Aoki, W., Kajino, T., et al. 2004, *ApJ*, 607, 474
- Iwamoto, N., Umeda, H., Tominaga, N., Nomoto, K., & Maeda, K. 2005, *Science*, 309, 451
- Johnson, J. A. & Bolte, M. 2002, *ApJ*, 579, 616
- Karlsson, T., Johnson, J. L., & Bromm, V. 2008, *ApJ*, 679, 6
- Keller, S. C., Bessell, M. S., Frebel, A., et al. 2014, *Nature*, 506, 463
- Kirby, E. N. & Cohen, J. G. 2012, *AJ*, 144, 168
- Kirby, E. N., Guhathakurta, P., Bolte, M., Sneden, C., & Geha, M. C. 2009, *ApJ*, 705, 328
- Kupka, F., Piskunov, N., Ryabchikova, T. A., Stempels, H. C., & Weiss, W. W. 1999, *A&AS*, 138, 119
- Lai, D. K., Lee, Y. S., Bolte, M., et al. 2011, *ApJ*, 738, 51
- Lee, Y. S., Beers, T. C., Masseron, T., et al. 2013, *AJ*, 146, 132
- Lucatello, S., Tsangarides, S., Beers, T. C., et al. 2005, *ApJ*, 625, 825
- Meynet, G., Ekström, S., & Maeder, A. 2006, *A&A*, 447, 623
- Mishenina, T. V., Kovtyukh, V. V., Soubiran, C., Travaglio, C., & Busso, M. 2002, *A&A*, 396, 189
- Norris, J. E., Ryan, S. G., & Beers, T. C. 2001, *ApJ*, 561, 1034
- Norris, J. E., Ryan, S. G., Beers, T. C., Aoki, W., & Ando, H. 2002, *ApJ*, 569, L107
- Norris, J. E., Yong, D., Bessell, M. S., et al. 2013, *ApJ*, 762, 28
- Pietrzyński, G., Gieren, W., Szewczyk, O., et al. 2008, *AJ*, 135, 1993
- Placco, V. M., Frebel, A., Beers, T. C., & Stancliffe, R. J. 2014, *ArXiv e-prints*
- Plez, B. 2012, *Turbospectrum: Code for spectral synthesis, astrophysics Source Code Library*
- Plez, B., Masseron, T., V., E., et al. 2007, in *Identification of near-UV predissociation lines of CH in carbon-enhanced Fe-poor stars, in Cool Star, Stellar Systems, and the Sun*, ed. G. van Belle, *ASP Conf. Series*, in press
- Preston, G. W. & Sneden, C. 2001, *AJ*, 122, 1545
- Querci, M., Querci, F., & Tsuji, T. 1972, in *Les Spectres des Astres dans l'Infrarouge et les Microondes*, 179–186
- Ramírez, I. & Meléndez, J. 2005, *ApJ*, 626, 465
- Salvadori, S. & Ferrara, A. 2009, *MNRAS*, 395, L6
- Salvadori, S. & Ferrara, A. 2012, *MNRAS*, 421, L29
- Salvadori, S., Schneider, R., & Ferrara, A. 2007, *MNRAS*, 381, 647
- Schlegel, D. J., Finkbeiner, D. P., & Davis, M. 1998, *ApJ*, 500, 525
- Shetrone, M., Venn, K. A., Tolstoy, E., et al. 2003, *AJ*, 125, 684
- Sivarani, T., Beers, T. C., Bonifacio, P., et al. 2006, *A&A*, 459, 125
- Sneden, C., Cowan, J. J., Lawler, J. E., et al. 2003, *ApJ*, 591, 936
- Sneden, C., Lucatello, S., Ram, R. S., Brooke, J. S. A., & Bernath, P. 2014, *ArXiv e-prints*
- Spite, M., Caffau, E., Andrievsky, S. M., et al. 2011, *A&A*, 528, A9
- Spite, M., Cayrel, R., Hill, V., et al. 2006, *A&A*, 455, 291
- Spite, M., Cayrel, R., Plez, B., et al. 2005, *A&A*, 430, 655
- Starkenburger, E., Hill, V., Tolstoy, E., et al. 2013, *A&A*, 549, A88
- Starkenburger, E., Shetrone, M. D., McConnachie, A. W., & Venn, K. A. 2014, *MNRAS*, 441, 1217
- Suda, T., Katsuta, Y., Yamada, S., et al. 2008, *PASJ*, 60, 1159
- Tafelmeyer, M., Jablonka, P., Hill, V., et al. 2010, *A&A*, 524, A58+
- Tolstoy, E., Hill, V., Irwin, M., et al. 2006, *The Messenger*, 123, 33
- Tolstoy, E., Hill, V., & Tosi, M. 2009, *ARA&A*, 47, 371
- Tominaga, N., Umeda, H., & Nomoto, K. 2007, *ApJ*, 660, 516
- Travaglio, C., Gallino, R., Arnone, E., et al. 2004, *ApJ*, 601, 864
- Tsujimoto, T. & Shigeyama, T. 2014, *A&A*, 565, L5
- Umeda, H. & Nomoto, K. 2003, *Nature*, 422, 871
- Woosley, S. E. & Weaver, T. A. 1995, *ApJS*, 101, 181
- Yong, D., Norris, J. E., Bessell, M. S., et al. 2013, *ApJ*, 762, 26

Table 4. Linelist and abundance measurements for individual lines. Errors are included for elements with fewer than five measured lines. A line where the abundance is marked with an hyphen, is fitted together with the previous line/lines.

X_i	λ	χ_{ex}	$\log(gf)$	$\log \epsilon(X_i)$	$\delta_{noise,i}$	Comment
Li I	6707.76	0.000	-0.009	< 0.17	-	blended
Li I	6707.91	0.000	-0.309	-	-	
O I	6300.30	0.000	-9.819	7.30	0.14	
O I	6363.78	0.020	-10.303	7.46	0.30	
Na I	5889.95	0.000	0.117	3.90	0.26	
Na I	5895.92	0.000	-0.184	3.68	0.20	
Na I	8183.26	2.102	0.230	3.94	0.28	
Mg I	4571.10	0.000	-5.691	6.02	-	
Mg I	4702.99	4.346	-0.666	5.80	-	
Mg I	5711.09	4.346	-1.833	5.96	-	
Mg I	8736.01	5.946	-3.210	6.04	-	
Mg I	8736.01	5.946	-1.930	-	-	
Mg I	8736.02	5.946	-3.300	-	-	
Mg I	8736.02	5.946	-0.690	-	-	
Mg I	8736.02	5.946	-1.970	-	-	
Mg I	8736.03	5.946	-1.020	-	-	
Mg I	8806.76	4.346	-0.137	6.02	-	
Al I	3961.52	0.014	-0.323	3.62	0.80	very blended
Si I	5708.40	4.954	-1.470	5.86	-	
Si I	5948.54	5.082	-1.230	5.80	-	blended
Si I	7034.90	5.871	-0.880	6.12	-	
Si I	7275.26	6.206	-7.048	5.90	-	blended
Si I	7275.26	6.206	-8.389	-	-	
Si I	7275.30	5.616	-0.847	-	-	
Si I	7409.08	5.616	-0.880	5.78	-	
Si I	7409.15	5.964	-1.566	-	-	
Si I	7423.50	5.619	-0.175	5.42	-	
Si I	8752.01	5.871	0.079	5.50	-	
S I	9212.86	6.525	0.420	5.42	0.32	
S I	9228.09	6.525	0.260	5.46	0.26	
K I	7664.91	0.000	0.130	3.46	0.10	
K I	7698.97	0.000	-0.170	3.44	0.06	
Ca I	5857.45	2.933	0.240	4.40	-	
Ca I	6102.44	2.523	-2.805	4.46	-	
Ca I	6102.72	1.879	-0.793	-	-	
Ca I	6122.22	1.886	-0.316	4.52	-	
Ca I	6161.30	2.523	-1.266	4.50	-	
Ca I	6162.17	1.899	-0.090	4.50	-	
Ca I	6166.44	2.521	-1.142	4.56	-	
Ca I	6169.04	2.523	-0.797	4.60	-	
Ca I	6169.56	2.526	-0.478	4.48	-	
Ca I	6439.08	2.526	0.390	4.44	-	
Ca I	6439.17	5.490	-3.709	-	-	
Ca I	6439.24	5.832	-4.094	-	-	
Ca I	6449.81	2.521	-0.502	4.48	-	
Ca I	6455.60	2.523	-1.340	4.56	-	blended
Ca I	6462.57	2.523	0.262	4.34	-	blended
Ca I	6471.66	2.526	-0.686	4.46	-	
Ca I	6493.78	2.521	-0.109	4.48	-	
Ca I	6499.65	2.523	-0.818	4.50	-	
Ca I	6572.78	0.000	-4.240	4.44	-	
Ca I	6717.68	2.709	-0.524	4.60	-	
Ca I	6717.69	5.883	-7.108	-	-	
Ca I	7148.15	2.709	0.137	4.58	-	
Ca I	7202.20	2.709	-0.262	4.44	-	
Ca I	7202.56	6.021	-4.660	-	-	
Ca I	7326.15	2.933	-0.208	4.42	-	
Ca I	7326.48	6.023	-5.128	-	-	
Ca I	7326.48	6.007	-4.670	-	-	
Sc II	4246.82	0.315	0.242	1.14	-	blended

Table 4. continued.

X_i	λ	χ_{ex}	$\log(gf)$	$\log \epsilon(X_i)$	$\delta_{noise,i}$	Comment
Sc II	4294.77	0.605	-1.391	0.90	-	very blended
Sc I	4320.62	2.109	-1.920	1.00	-	blended
Sc II	4320.73	0.605	-0.252	-	-	
Sc I	4415.48	3.083	-3.393	1.24	-	blended
Sc II	4415.56	0.595	-0.668	-	-	
Sc I	4431.23	1.851	-6.387	1.16	-	
Sc II	4431.35	0.605	-1.969	-	-	
Sc I	4431.52	3.083	-2.584	-	-	
Sc II	4670.41	1.357	-0.576	0.92	-	very blended
Sc I	4670.52	3.172	-2.584	-	-	
Sc II	6245.64	1.507	-1.030	1.24	-	blended
Sc I	6279.57	3.607	-1.673	1.18	-	
Sc II	6279.75	1.500	-1.265	-	-	
Sc II	6604.60	1.357	-1.309	1.16	-	
Ti II	4493.51	1.080	-3.020	3.12	-	
Ti II	4501.27	1.116	-0.770	2.78	-	
Ti I	4562.63	0.021	-2.656	3.00	-	
Ti I	4563.42	2.427	-0.681	2.92	-	
Ti II	4563.76	1.221	-0.690	-	-	
Ti II	4568.31	1.224	-2.940	3.08	-	
Ti II	4583.41	1.165	-2.920	3.18	-	
Ti II	4609.26	1.180	-3.430	3.26	-	
Ti I	4609.34	3.319	-2.072	-	-	
Ti I	4617.27	1.749	0.389	2.96	-	
Ti I	4708.42	3.199	-3.799	3.18	-	blended
Ti I	4708.43	1.873	-6.885	-	-	
Ti II	4708.66	1.237	-2.340	-	-	
Ti I	4759.14	2.778	-2.543	3.12	-	
Ti I	4759.27	2.256	0.514	-	-	
Ti II	4764.52	1.237	-2.950	3.50	-	
Ti I	4792.25	0.813	-3.468	3.28	-	blended
Ti II	4792.43	1.237	-3.328	-	-	
Ti I	4792.48	2.334	-0.300	-	-	
Ti II	4805.08	2.061	-0.960	3.14	-	
Ti I	4805.42	2.345	0.150	-	-	
Ti I	4805.44	3.062	-3.409	-	-	
Ti I	4840.87	0.900	-0.509	3.04	-	
Ti II	4865.61	1.116	-2.790	3.32	-	
Ti I	4865.78	2.578	-0.398	-	-	
Ti III	4874.00	18.252	0.560	3.12	-	
Ti II	4874.01	3.095	-0.800	-	-	
Ti I	4885.08	1.887	0.358	2.96	-	blended
Ti I	4885.20	2.677	-1.681	-	-	
Ti I	4913.46	2.506	-3.499	3.18	-	
Ti I	4913.61	1.873	0.160	-	-	
Ti I	4981.73	0.848	0.504	2.88	-	
Ti I	4981.90	2.427	-3.637	-	-	
Ti I	5866.23	3.176	-3.522	3.12	-	
Ti I	5866.37	3.305	-0.186	-	-	
Ti I	5866.45	1.067	-0.840	-	-	
Ti II	5866.66	8.089	-0.620	-	-	
Ti II	5899.03	8.082	-2.325	3.16	-	
Ti I	5899.29	1.053	-1.154	-	-	
Ti I	5899.50	3.351	-2.307	-	-	
Ti I	5921.92	3.691	-2.186	3.22	-	
Ti II	5921.94	8.056	-0.024	-	-	
Ti I	5922.11	1.046	-1.466	-	-	
Ti I	5922.14	3.113	-1.602	-	-	
Ti II	5952.98	8.071	-0.063	3.00	-	
Ti I	5953.11	3.090	-3.612	-	-	
Ti I	5953.16	1.887	-0.329	-	-	

Table 4. continued.

X_i	λ	χ_{ex}	$\log(gf)$	$\log \epsilon(X_i)$	$\delta_{noise,i}$	Comment
Ti I	5965.32	3.409	-3.412	3.14	-	blended
Ti II	5965.81	8.089	-1.623	-	-	
Ti I	5965.83	1.879	-0.409	-	-	
Ti II	5978.41	8.093	-0.535	3.14	-	
Ti I	5978.54	1.873	-0.496	-	-	
Ti II	6126.00	8.097	-1.650	3.22	-	
Ti I	6126.22	1.067	-1.425	-	-	
Ti I	6126.27	3.154	-3.025	-	-	
Ti I	6257.80	0.000	-4.297	3.04	-	
Ti I	6258.10	1.443	-0.355	-	-	
Ti I	6258.71	1.460	-0.240	3.14	-	
Ti I	6261.10	1.430	-0.479	3.16	-	
Ti I	6261.12	3.128	-1.798	-	-	
Ti I	6261.28	3.323	-3.656	-	-	
Ti II	6491.56	2.061	-1.793	2.98	-	
Ti I	6556.06	1.460	-1.074	3.38	-	
Ti II	6559.59	2.048	-2.019	3.04	-	
Ti I	7209.44	1.460	-0.500	3.14	-	blended
Ti I	7209.62	3.424	-1.599	-	-	
Ti I	7244.85	1.443	-0.810	3.24	-	blended
Ti I	7251.71	1.430	-0.770	3.02	-	blended
V II	4002.80	1.555	-5.601	2.14	-	
V II	4002.94	1.428	-1.447	-	-	
V I	4003.01	2.332	-3.063	-	-	
V I	4003.12	2.359	-4.625	-	-	
V I	4003.13	2.505	-9.645	-	-	
V I	4003.17	2.578	-1.161	-	-	
V I	4586.23	2.578	-6.028	1.88	-	
V I	4586.37	0.040	-0.790	-	-	
V I	4586.44	1.376	-6.348	-	-	
V I	4586.55	2.505	-3.017	-	-	
V I	4827.46	0.040	-1.478	1.94	-	
V II	4827.47	8.645	-3.405	-	-	
V I	4827.54	2.040	-5.969	-	-	
V I	4827.69	2.878	-3.382	-	-	
V I	4831.65	0.017	-1.380	1.96	-	
V I	4831.77	1.955	-3.283	-	-	
V I	4864.73	0.017	-0.960	1.78	-	
V I	4864.83	1.183	-1.240	-	-	
V II	4864.87	6.857	-2.457	-	-	
V II	4875.22	6.547	-4.285	1.98	-	
V I	4875.42	1.351	-4.161	-	-	
V I	4875.49	0.040	-0.810	-	-	
V II	4875.50	5.468	-1.533	-	-	
V II	4875.62	4.005	-3.268	-	-	
V I	5703.58	1.051	-0.211	2.20	-	
V II	5703.65	3.973	-4.727	-	-	
V II	5706.77	6.901	-3.971	2.18	-	
V II	5706.86	9.031	-1.107	-	-	
V I	5706.98	1.043	-0.454	-	-	
V I	6039.72	1.064	-0.650	2.10	-	
V I	6039.86	3.517	-2.920	-	-	
V I	6039.86	2.555	-4.421	-	-	
V I	6090.21	1.081	-0.062	1.98	-	
V II	6090.47	3.799	-6.833	-	-	
V I	6090.54	1.064	-2.600	-	-	
Cr II	4545.94	8.348	-2.289	2.96	-	
Cr I	4545.95	0.941	-1.370	-	-	
Cr I	4546.02	3.551	-3.528	-	-	
Cr II	4546.03	6.805	-3.416	-	-	
Cr II	4588.20	4.071	-0.845	3.84	-	

Table 4. continued.

X_i	λ	χ_{ex}	$\log(gf)$	$\log \epsilon(X_i)$	$\delta_{noise,i}$	Comment
Cr I	4588.24	4.389	-3.887	-	-	
Cr II	4588.40	3.104	-4.542	-	-	
Cr I	4591.13	4.402	-3.455	3.34	-	
Cr I	4591.39	0.968	-1.740	-	-	
Cr II	4591.42	10.599	-4.794	-	-	
Cr I	4591.46	4.440	-1.925	-	-	
Cr I	4591.48	3.422	-1.888	-	-	
Cr I	4591.60	4.490	-3.992	-	-	
Cr I	4616.12	0.983	-1.190	3.18	-	
Cr II	4616.24	5.670	-2.346	-	-	
Cr I	4625.92	3.850	-0.310	3.26	-	
Cr II	4625.94	11.677	-0.760	-	-	
Cr I	4626.02	4.532	-0.960	-	-	
Cr II	4626.09	11.788	-4.123	-	-	
Cr I	4626.17	0.968	-1.320	-	-	
Cr I	4634.00	3.551	-1.808	3.70	-	blended
Cr II	4634.07	4.072	-1.236	-	-	
Cr II	4651.13	11.622	-1.756	3.44	-	
Cr II	4651.23	10.243	-5.278	-	-	
Cr I	4651.28	0.983	-1.460	-	-	
Cr II	4651.40	11.711	-3.420	-	-	
Cr II	4652.04	10.476	-1.599	3.32	-	
Cr I	4652.16	1.004	-1.030	-	-	
Cr II	4652.27	5.871	-4.565	-	-	
Cr II	4755.95	7.899	-5.302	3.84	-	
Cr I	4756.05	2.987	-2.912	-	-	
Cr I	4756.11	3.104	0.090	-	-	
Cr I	4756.16	4.106	-3.511	-	-	
Cr I	4756.31	4.411	-4.185	-	-	
Cr II	4829.18	10.476	-2.906	3.96	-	
Cr II	4829.22	10.798	-2.554	-	-	
Cr I	4829.22	3.369	-2.423	-	-	
Cr I	4829.31	2.545	-1.604	-	-	
Cr I	4829.37	2.545	-0.810	-	-	
Cr I	4848.06	5.211	-1.253	3.70	-	
Cr II	4848.23	3.864	-1.280	-	-	
Cr I	4876.40	4.096	-2.973	3.76	-	
Cr II	4876.40	3.854	-1.580	-	-	
Cr II	4876.47	3.864	-2.093	-	-	
Cr II	4876.67	6.686	-2.966	-	-	
Cr II	4876.69	8.363	-6.334	-	-	
Cr I	4922.16	3.435	-3.337	3.50	-	
Cr II	4922.22	10.843	-2.464	-	-	
Cr I	4922.27	3.104	0.270	-	-	
Cr II	4922.36	10.454	-2.474	-	-	
Cr I	4922.54	3.011	-2.173	-	-	
Cr I	4942.50	0.941	-2.294	3.58	-	
Cr I	4942.75	3.449	-3.467	-	-	
Cr I	4964.93	0.941	-2.527	3.58	-	
Cr II	4965.00	8.354	-5.841	-	-	
Cr I	6330.09	0.941	-2.920	3.56	-	
Cr II	6330.40	11.144	-1.000	-	-	
Mn I	4055.54	2.143	-0.070	3.06	-	blended
Mn III	4079.03	11.095	-9.881	2.88	-	very blended
Mn III	4079.18	23.795	-0.432	-	-	
Mn I	4079.22	4.258	-0.161	-	-	
Mn I	4079.24	2.143	-0.530	-	-	
Mn I	4079.41	2.187	-0.420	-	-	
Mn II	4753.74	6.528	-4.469	3.30	-	
Mn I	4753.89	5.214	-0.965	-	-	
Mn II	4754.03	10.271	-3.379	-	-	

Table 4. continued.

X_i	λ	χ_{ex}	$\log(gf)$	$\log \epsilon(X_i)$	$\delta_{noise,i}$	Comment
Mn I	4754.04	2.282	-0.086	-	-	
Mn II	4754.06	6.139	-3.081	-	-	
Mn I	4762.37	2.888	0.425	2.94	-	blended
Mn III	4765.84	14.459	-4.448	3.22	-	
Mn I	4765.85	2.941	-0.080	-	-	
Mn I	4766.00	4.425	-1.730	-	-	
Mn III	4766.29	24.215	-1.865	3.16	-	
Mn I	4766.42	2.920	0.100	-	-	
Mn III	4766.46	21.564	-2.589	-	-	
Mn II	4766.52	10.661	-4.115	-	-	
Mn I	4766.66	5.199	-0.560	-	-	
Mn II	4783.29	10.283	-4.252	3.32	-	
Mn I	4783.43	2.298	0.042	-	-	
Mn I	4823.52	2.319	0.144	3.30	-	blended
Mn II	4823.65	11.683	-2.969	-	-	
Mn I	6013.51	3.072	-0.251	3.00	-	
Fe I	5762.84	4.301	-2.620	5.48	-	
Fe I	5762.98	4.191	-3.199	-	-	
Fe I	5762.99	4.209	-0.450	-	-	
Fe I	5763.00	4.191	-4.561	-	-	
Fe I	5862.23	3.640	-4.359	5.30	-	
Fe I	5862.36	4.549	-0.127	-	-	
Fe I	5862.47	5.334	-3.802	-	-	
Fe I	5914.11	4.608	-0.375	5.34	-	
Fe I	5914.20	4.608	-0.131	-	-	
Fe I	5956.41	5.352	-5.829	5.68	-	
Fe I	5956.46	4.283	-4.169	-	-	
Fe I	5956.51	5.352	-8.937	-	-	
Fe I	5956.69	0.859	-4.605	-	-	
Fe I	5956.94	4.580	-3.540	-	-	
Fe I	5976.69	5.330	-5.182	5.44	-	
Fe I	5976.78	3.943	-1.243	-	-	
Fe I	6002.77	5.314	-3.755	5.58	-	
Fe I	6002.79	5.386	-4.886	-	-	
Fe I	6003.01	3.881	-1.120	-	-	
Fe I	6003.02	5.506	-7.385	-	-	
Fe I	6003.11	5.506	-7.472	-	-	
Fe I	6003.11	5.506	-8.111	-	-	
Fe I	6003.17	5.506	-7.907	-	-	
Fe I	6055.76	5.352	-7.003	5.58	-	
Fe I	6055.78	5.357	-7.928	-	-	
Fe I	6055.89	5.352	-7.777	-	-	
Fe I	6055.94	5.070	-2.322	-	-	
Fe I	6055.94	5.352	-5.833	-	-	
Fe I	6055.95	5.357	-6.627	-	-	
Fe I	6055.95	5.357	-8.619	-	-	
Fe I	6056.01	4.733	-0.460	-	-	
Fe I	6056.09	5.357	-7.290	-	-	
Fe I	6056.09	5.357	-7.768	-	-	
Fe I	6056.25	5.357	-7.202	-	-	
Fe I	6065.48	2.608	-1.530	5.48	-	
Fe I	6065.49	4.956	-3.471	-	-	
Fe I	6082.46	5.486	-8.673	5.54	-	
Fe I	6082.54	5.386	-5.272	-	-	
Fe I	6082.58	5.607	-9.656	-	-	
Fe I	6082.58	5.607	-3.403	-	-	
Fe I	6082.61	4.220	-3.746	-	-	
Fe I	6082.71	2.223	-3.573	-	-	
Fe I	6082.85	5.341	-3.667	-	-	
Fe I	6082.89	5.486	-8.142	-	-	
Fe I	6082.89	5.486	-9.294	-	-	

Table 4. continued.

X_i	λ	χ_{ex}	$\log(gf)$	$\log \epsilon(X_i)$	$\delta_{noise,i}$	Comment
Fe I	6136.25	5.273	-3.556	5.48	-	-
Fe I	6136.62	2.453	-1.400	-	-	-
Fe I	6136.99	2.198	-2.950	-	-	-
Fe I	6137.28	4.580	-2.160	-	-	-
Fe I	6137.47	4.301	-3.741	-	-	-
Fe I	6137.50	3.332	-2.514	-	-	-
Fe I	6137.69	2.588	-1.403	-	-	-
Fe I	6151.62	2.176	-3.299	5.58	-	-
Fe I	6151.69	5.012	-3.761	-	-	-
Fe I	6173.01	0.990	-7.794	5.62	-	-
Fe I	6173.03	3.640	-4.961	-	-	-
Fe I	6173.15	4.991	-3.920	-	-	-
Fe I	6173.29	5.372	-5.600	-	-	-
Fe I	6173.33	2.223	-2.880	-	-	-
Fe I	6173.34	5.334	-4.314	-	-	-
Fe I	6173.49	5.348	-7.269	-	-	-
Fe I	6173.64	4.446	-3.400	-	-	-
Fe I	6180.20	2.727	-2.586	5.52	-	-
Fe I	6180.29	5.314	-4.453	-	-	-
Fe I	6191.56	2.433	-1.417	5.30	-	-
Fe I	6191.57	4.256	-5.483	-	-	-
Fe I	6191.77	4.143	-5.123	-	-	-
Fe I	6200.27	4.320	-3.931	5.54	-	-
Fe I	6200.31	2.608	-2.437	-	-	-
Fe I	6200.51	5.357	-9.018	-	-	-
Fe I	6213.27	5.386	-4.197	5.52	-	-
Fe I	6213.43	2.223	-2.482	-	-	-
Fe I	6218.94	5.446	-8.948	5.56	-	-
Fe I	6219.14	5.010	-2.270	-	-	-
Fe I	6219.28	2.198	-2.433	-	-	-
Fe I	6219.31	5.458	-5.082	-	-	-
Fe I	6219.53	3.417	-4.100	-	-	-
Fe I	6219.58	5.345	-4.691	-	-	-
Fe I	6230.48	5.410	-5.491	5.44	-	-
Fe I	6230.72	2.559	-1.281	-	-	-
Fe I	6252.38	4.320	-7.012	5.48	-	-
Fe I	6252.56	2.404	-1.687	-	-	-
Fe I	6252.78	5.648	-8.652	-	-	-
Fe I	6254.26	2.279	-2.443	5.58	-	-
Fe I	6301.50	3.654	-0.718	5.38	-	-
Fe I	6301.77	5.458	-2.889	-	-	-
Fe I	6317.76	5.314	-5.205	5.76	-	-
Fe I	6318.02	2.453	-2.261	-	-	-
Fe I	6318.04	5.683	-9.049	-	-	-
Fe I	6318.05	5.683	-5.610	-	-	-
Fe I	6318.05	5.683	-8.040	-	-	-
Fe I	6318.35	5.314	-5.989	-	-	-
Fe I	6322.69	2.588	-2.426	5.54	-	-
Fe I	6322.74	5.491	-5.869	-	-	-
Fe I	6335.33	2.198	-2.177	5.44	-	-
Fe I	6344.02	4.415	-3.572	5.64	-	-
Fe I	6344.07	5.524	-8.598	-	-	-
Fe I	6344.08	5.524	-6.712	-	-	-
Fe I	6344.15	2.433	-2.923	-	-	-
Fe I	6344.28	5.486	-8.925	-	-	-
Fe I	6344.28	4.473	-6.227	-	-	-
Fe I	6344.37	5.486	-9.075	-	-	-
Fe I	6344.37	5.486	-8.548	-	-	-
Fe I	6358.43	4.593	-3.620	5.76	-	-
Fe I	6358.51	5.388	-4.570	-	-	-
Fe I	6358.63	5.345	-5.414	-	-	-

Table 4. continued.

X_i	λ	χ_{ex}	$\log(gf)$	$\log \epsilon(X_i)$	$\delta_{noise,i}$	Comment
Fe I	6358.63	4.143	-1.657	-	-	
Fe I	6358.65	4.371	-3.448	-	-	
Fe I	6358.70	0.859	-4.468	-	-	
Fe I	6399.53	5.669	-9.756	5.46	-	
Fe I	6399.61	5.669	-8.100	-	-	
Fe I	6399.61	5.669	-9.605	-	-	
Fe I	6399.65	3.984	-3.287	-	-	
Fe I	6399.69	5.502	-5.292	-	-	
Fe I	6399.77	5.669	-9.938	-	-	
Fe I	6399.79	5.357	-6.843	-	-	
Fe I	6399.85	5.502	-6.988	-	-	
Fe I	6400.00	3.602	-0.290	-	-	
Fe I	6400.06	5.314	-4.911	-	-	
Fe I	6400.13	5.669	-7.575	-	-	
Fe I	6400.32	0.915	-4.318	-	-	
Fe I	6400.34	5.064	-3.635	-	-	
Fe I	6400.37	5.502	-7.493	-	-	
Fe I	6400.37	5.502	-8.377	-	-	
Fe I	6411.65	3.654	-0.595	5.42	-	
Fe I	6411.99	5.446	-5.559	-	-	
Fe I	6421.21	5.334	-3.994	5.52	-	
Fe I	6421.35	2.279	-2.027	-	-	
Fe I	6421.57	5.334	-5.293	-	-	
Fe I	6494.98	2.404	-1.273	5.34	-	
Fe I	6545.85	4.580	-3.977	5.30	-	
Fe I	6545.99	5.314	-3.547	-	-	
Fe I	6546.20	5.357	-7.253	-	-	
Fe I	6546.24	2.758	-1.536	-	-	
Fe I	6546.47	5.841	-7.040	-	-	
Fe I	6546.50	4.473	-6.658	-	-	
Fe I	6592.61	4.956	-1.262	5.30	-	
Fe I	6592.91	2.727	-1.473	-	-	
Fe I	6593.87	2.433	-2.422	5.50	-	
Fe I	6608.03	2.279	-4.030	5.52	-	
Fe I	7494.72	1.557	-5.254	5.26	-	
Fe I	7494.84	5.458	-3.505	-	-	
Fe I	7494.90	4.985	-3.470	-	-	
Fe I	7495.00	3.695	-6.916	-	-	
Fe I	7495.01	5.720	-2.463	-	-	
Fe I	7495.07	4.220	0.053	-	-	
Fe I	7495.37	5.693	-3.673	-	-	
Fe I	7664.16	4.835	-1.176	5.42	-	
Fe I	7664.29	2.990	-1.683	-	-	
Fe I	7664.42	5.849	-2.832	-	-	
Fe I	7664.45	4.733	-3.527	-	-	
Fe I	7722.91	5.539	-5.064	5.78	-	
Fe I	7723.21	2.279	-3.617	-	-	
Fe I	7723.54	5.793	-4.026	-	-	
Fe I	7723.59	5.539	-5.366	-	-	
Fe I	7780.23	5.519	-3.671	5.24	-	
Fe I	7780.51	5.683	-3.647	-	-	
Fe I	7780.56	4.473	0.029	-	-	
Fe I	7780.59	5.693	-4.952	-	-	
Fe I	7780.75	5.930	-8.656	-	-	
Fe I	7831.86	5.386	-4.697	5.34	-	
Fe I	7832.20	4.435	0.111	-	-	
Fe I	8046.05	4.415	0.031	5.28	-	
Fe I	8387.77	2.176	-1.493	5.42	-	
Fe I	8387.96	5.879	-7.512	-	-	
Fe I	8388.07	5.642	-3.588	-	-	
Fe I	8515.11	3.018	-2.073	5.66	-	

Table 4. continued.

X_i	λ	χ_{ex}	$\log(gf)$	$\log \epsilon(X_i)$	$\delta_{noise,i}$	Comment
Fe I	8621.60	2.949	-2.321	5.46	-	
Fe I	8621.89	5.967	-7.684	-	-	
Fe I	8674.31	5.720	-6.667	5.58	-	
Fe I	8674.36	6.010	-7.879	-	-	
Fe I	8674.54	5.996	-8.466	-	-	
Fe I	8674.58	5.621	-6.068	-	-	
Fe I	8674.58	5.693	-4.781	-	-	
Fe I	8674.75	2.831	-1.800	-	-	
Fe I	8675.19	5.913	-5.414	-	-	
Fe I	8763.97	4.652	-0.146	5.38	-	
Fe I	8975.11	5.979	-5.119	5.48	-	
Fe I	8975.16	4.988	-2.087	-	-	
Fe I	8975.27	3.686	-7.036	-	-	
Fe I	8975.31	4.143	-4.759	-	-	
Fe I	8975.40	2.990	-2.233	-	-	
Fe I	8975.42	5.883	-5.666	-	-	
Fe I	8975.69	5.334	-6.162	-	-	
Fe I	8975.80	5.352	-8.779	-	-	
Fe I	8999.56	2.831	-1.321	5.40	-	
Fe I	9088.03	5.502	-4.483	5.40	-	
Fe I	9088.32	2.845	-1.986	-	-	
Fe I	9088.35	5.930	-5.925	-	-	
Fe I	9088.46	6.010	-5.111	-	-	
Fe I	9088.50	5.928	-3.861	-	-	
Fe I	9089.40	2.949	-1.675	-	-	
Fe I	9089.50	5.947	-4.040	-	-	
Fe I	9145.78	6.252	-9.640	5.22	-	
Fe I	9145.80	5.693	-5.595	-	-	
Fe I	9146.13	2.588	-2.804	-	-	
Fe II	6247.14	11.164	-4.093	5.70	0.14	blended
Fe II	6247.26	11.237	-4.082	-	-	
Fe II	6247.35	6.209	-2.172	-	-	
Fe II	6247.37	10.909	-1.382	-	-	
Fe II	6247.44	12.276	-5.381	-	-	
Fe II	6247.56	3.892	-2.435	-	-	
Fe II	6247.57	5.956	-4.827	-	-	
Fe II	6247.66	11.591	-8.222	-	-	
Fe II	6432.47	10.448	-9.829	5.72	0.10	blended
Fe II	6432.68	10.930	-1.236	-	-	
Fe II	6432.68	2.891	-3.687	-	-	
Fe II	6456.38	3.903	-2.185	5.64	0.12	blended
Fe II	6456.47	11.547	-4.091	-	-	
Fe II	6516.08	2.891	-3.432	5.56	0.08	blended
Co I	4233.71	3.930	-3.106	3.02	-	
Co I	4233.98	0.000	-3.469	-	-	
Co I	4813.45	2.871	-2.121	3.28	-	
Co I	4813.47	3.216	0.050	-	-	
Co 4	4813.71	17.943	-6.686	-	-	
Co II	4840.10	11.326	-2.988	3.16	-	
Co I	4840.25	3.170	0.144	-	-	
Co II	4840.37	3.459	-5.518	-	-	
Co I	6450.08	2.137	-2.132	2.96	-	
Co I	6450.25	1.710	-1.698	-	-	
Co I	6872.39	2.008	-1.589	2.80	-	
Co I	7052.87	1.956	-1.264	2.58	-	
Co I	7084.98	1.883	-1.018	2.62	-	
Ni I	5711.88	1.935	-2.270	4.18	-	blended
Ni I	5715.07	4.088	-0.352	4.22	-	blended
Ni II	5748.25	14.896	-0.858	4.10	-	
Ni I	5748.35	1.676	-3.260	-	-	
Ni I	5754.51	3.941	-3.611	4.38	-	

Table 4. continued.

X_i	λ	χ_{ex}	$\log(gf)$	$\log \epsilon(X_i)$	$\delta_{noise,i}$	Comment
Ni II	5754.51	14.733	-2.531	-	-	
Ni I	5754.65	1.935	-2.330	-	-	
Ni III	5754.87	22.952	-2.744	-	-	
Ni II	5846.77	12.208	-3.583	4.14	-	
Ni I	5846.99	1.676	-3.210	-	-	
Ni I	5892.75	4.154	-1.494	4.32	-	blended
Ni I	5892.87	1.986	-2.350	-	-	
Ni II	5892.94	14.667	-2.139	-	-	
Ni II	5893.25	15.008	-1.827	-	-	
Ni I	6007.31	1.676	-3.330	4.14	-	
Ni II	6007.35	13.080	-1.934	-	-	
Ni I	6108.11	1.676	-2.450	4.06	-	
Ni I	6116.17	4.089	-0.677	4.26	-	
Ni I	6116.17	4.266	-0.822	-	-	
Ni II	6116.20	15.026	-2.610	-	-	
Ni I	6128.96	1.676	-3.330	4.18	-	
Ni II	6176.62	15.008	-2.753	4.16	-	
Ni I	6176.81	4.088	-0.260	-	-	
Ni I	6177.24	1.826	-3.500	-	-	
Ni II	6177.28	11.969	-3.167	-	-	
Ni I	6177.54	4.236	-2.141	-	-	
Ni II	6314.46	12.904	0.480	3.62	-	
Ni II	6314.48	14.903	-1.870	-	-	
Ni I	6314.65	1.935	-1.770	-	-	
Ni I	6314.66	4.154	-0.921	-	-	
Ni II	6314.73	14.906	-2.400	-	-	
Ni II	6327.37	12.457	-3.303	4.14	-	
Ni II	6327.54	14.837	-3.471	-	-	
Ni I	6327.59	1.676	-3.150	-	-	
Ni II	6327.71	14.685	-1.895	-	-	
Ni II	6327.79	15.022	-1.043	-	-	
Ni II	6482.67	14.912	-1.094	3.94	-	
Ni II	6482.67	14.912	-1.010	-	-	
Ni I	6482.80	1.935	-2.630	-	-	
Ni II	6482.81	14.744	-1.692	-	-	
Ni II	6482.82	14.744	-1.185	-	-	
Ni II	6482.91	14.912	-2.596	-	-	
Ni II	6482.94	14.912	-2.779	-	-	
Ni II	6483.02	14.912	-2.258	-	-	
Ni II	6483.03	14.912	-2.782	-	-	
Ni II	6586.26	14.739	-2.772	4.10	-	
Ni I	6586.31	1.951	-2.810	-	-	
Ni II	6643.40	14.731	-3.243	4.26	-	
Ni I	6643.63	1.676	-2.300	-	-	
Ni II	6767.54	15.224	-2.851	4.20	-	
Ni I	6767.77	1.826	-2.170	-	-	
Ni I	6914.56	1.951	-2.270	4.12	-	
Ni I	7197.01	1.935	-2.680	4.28	-	blended
Ni II	7197.25	14.334	-2.630	-	-	
Ni I	7197.39	5.004	-3.128	-	-	
Ni II	7393.23	15.059	-1.426	4.70	-	blended
Ni I	7393.60	3.606	-0.825	-	-	
Ni II	7408.96	14.486	-3.296	4.04	-	blended
Ni II	7409.01	14.473	-2.127	-	-	
Ni I	7409.04	5.497	-2.476	-	-	
Ni I	7409.25	5.514	-1.790	-	-	
Ni I	7409.35	3.796	-0.237	-	-	
Ni I	7414.50	1.986	-2.570	4.32	-	blended
Cu I	5782.13	1.642	-1.720	1.44	0.26	
Zn I	4680.13	4.006	-0.815	2.82	0.26	blended
Zn I	4722.15	4.030	-0.338	2.60	0.26	blended

Table 4. continued.

X_i	λ	χ_{ex}	$\log(gf)$	$\log \epsilon(X_i)$	$\delta_{noise,i}$	Comment
Zn I	4810.53	4.078	-0.137	2.64	0.20	
Ga I	4172.04	0.102	-0.270	0.82	0.44	very blended
Sr II	4077.71	0.000	0.167	1.44	0.34	very blended
Sr I	4607.33	0.000	-0.570	1.70	0.16	
Y II	4682.32	0.409	-1.510	0.70	-	blended
Y II	4823.30	0.992	-1.110	0.56	-	blended
Y II	4854.86	0.992	-0.380	0.60	-	
Y II	4883.68	1.084	0.070	0.50	-	
Y I	4900.08	1.398	-0.360	0.52	-	blended
Y II	4900.12	1.033	-0.090	-	-	
Y I	4981.97	1.983	-1.980	0.44	-	
Y II	4982.13	1.033	-1.290	-	-	
Zr II	3998.95	0.559	-0.520	1.08	-	blended
Zr II	4029.68	0.713	-0.780	0.98	-	blended
Zr II	4258.04	0.559	-1.200	0.74	-	blended
Zr II	4317.30	0.713	-1.450	0.92	-	
Zr II	4613.95	0.972	-1.540	0.98	-	
Ba II	4554.03	0.000	0.170	-0.34	-	blended
Ba II	4934.08	0.000	-0.150	-0.32	-	blended
Ba II	5853.67	0.604	-1.000	-0.48	-	
Ba II	6141.71	0.704	-0.076	-0.44	-	
Ba II	6496.90	0.604	-0.377	-0.14	-	
La II	3988.51	0.403	0.170	-1.34	-	
La II	3995.75	0.173	-0.100	-1.00	-	blended
La II	4031.69	0.321	-0.090	-0.96	-	very blended
La II	4086.71	0.000	-0.070	-1.24	-	very blended
La II	4123.22	0.321	0.110	-0.54	-	very blended
La II	4333.75	0.173	-0.060	-0.80	-	very blended
La II	4662.50	0.000	-1.240	-1.12	-	
La II	4740.28	0.126	-1.050	-1.06	-	blended
La II	4920.98	0.126	-0.580	-1.46	-	blended
La II	4921.78	0.244	-0.450	-1.26	-	blended
Ce II	4053.50	0.000	-0.710	-0.62	-	very blended
Ce II	4053.53	0.621	-2.740	-	-	
Ce II	4053.57	3.469	-2.910	-	-	
Ce II	4053.59	1.048	-1.490	-	-	
Ce II	4418.78	0.864	0.280	-0.20	-	
Ce II	4483.89	0.864	0.150	-0.22	-	blended
Ce III	4484.06	12.490	-1.860	-	-	
Ce II	4486.88	1.339	-1.200	-0.56	-	
Ce II	4486.91	0.295	-0.260	-	-	
Ce II	4487.00	3.562	-1.100	-	-	
Ce II	4487.12	0.122	-3.350	-	-	
Ce II	4487.17	0.232	-2.540	-	-	
Ce II	4539.42	1.930	-0.810	-1.18	-	blended
Ce II	4539.50	1.042	-3.320	-	-	
Ce II	4539.58	0.900	-1.060	-	-	
Ce II	4539.61	1.412	-0.910	-	-	
Ce II	4539.75	0.328	-0.020	-	-	
Ce II	4539.85	1.645	-2.050	-	-	
Ce II	4562.28	1.327	-2.120	-0.92	-	
Ce II	4562.36	0.478	0.230	-	-	
Ce II	4572.28	0.684	0.290	-0.56	-	blended
Ce II	4628.16	0.516	0.200	-0.68	-	
Ce II	4628.19	1.194	-3.280	-	-	
Ce II	4628.24	1.366	-0.430	-	-	
Pr II	4408.82	0.000	-0.278	< -1.30	-	blended
Pr II	4408.82	0.000	-0.278	< -1.10	-	blended
Nd II	4004.00	0.064	-0.570	-0.58	-	blended
Nd II	4021.33	0.321	-0.100	-0.74	-	
Nd II	4351.28	0.182	-0.610	-0.40	-	very blended

Table 4. continued.

X_i	λ	χ_{ex}	$\log(gf)$	$\log \epsilon(X_i)$	$\delta_{noise,i}$	Comment
Nd II	4446.38	0.205	-0.350	-0.84	-	
Nd II	4506.58	0.064	-1.040	-0.88	-	blended
Nd II	4811.34	0.064	-1.015	-0.38	-	
Nd II	4825.48	0.182	-0.420	-0.62	-	
Nd II	4859.03	0.321	-0.440	-0.62	-	
Nd II	4959.12	0.064	-0.800	-0.44	-	
Nd II	6900.44	0.000	-1.542	-0.60	-	
Sm II	4318.93	0.277	-0.250	-1.02	0.50	blended
Sm II	4434.32	0.378	-0.070	-0.66	0.32	blended
Sm II	4467.34	0.659	0.150	-1.04	0.26	blended
Eu II	3907.11	0.207	0.170	-1.72	0.38	very blended
Eu II	4129.72	0.000	0.220	-1.44	0.38	very blended
Eu II	4205.04	0.000	0.210	-1.66	0.66	very blended
Eu II	4435.58	0.207	-0.110	-1.22	0.40	very blended
Eu II	6645.06	1.380	0.120	< -1.22	-	
Gd II	4251.73	0.382	-0.220	< -0.50	-	
Tb II	4752.53	0.000	-0.550	< -1.38	-	blended
Dy II	3944.68	0.000	0.110	-0.86	0.50	very blended
Dy II	3983.65	0.538	-0.310	< -0.38	-	very blended
Dy II	4103.31	0.103	-0.380	-1.00	0.56	very blended
Dy II	4449.70	0.000	-1.030	< -0.66	-	very blended
Er II	3896.23	0.055	-0.241	< -0.60	-	very blended
Pb I	4057.81	1.320	-0.170	< 0.92	-	very blended
Th II	4250.34	0.557	0.000	< -1.20	-	blended

Table 6. Carbon estimates and upper limits from CN molecular lines in the wavelength range 9100-9250 Å (VLT/FLAMES). The estimates, $[C/Fe]_{\text{est}}$, are measured by assuming $[C/N] = -1.2$, the average value for mixed stars in the range $-3 \leq [Fe/H] \leq -2$ (Spite et al. 2005). The upper limits, $[C/Fe]_{\text{lim}}$, are measured by assuming $[N/Fe] = 0$, while all mixed stars in Spite et al. (2005) have $[N/Fe] > 0.5$. This lower limit of N therefore gives an upper limit of C. In both cases a simple relation of oxygen with $[Fe/H]$, as shown in Fig. 6a, is assumed for stars that do not have known oxygen values. Iron values, luminosities, and oxygen measurements, when available, are obtained from Hill et al. in prep. The solar values are adopted from Grevesse & Sauval (1998).

Star	RA	DEC	$\log L_*/L_\odot$	[Fe/H]	$[C/Fe]_{\text{est}}$	$[C/Fe]_{\text{lim}}$
ET0024	1 00 34.04	-33 39 04.6	3.26	-1.24	-0.94	-0.74
ET0026	1 00 12.76	-33 41 16.0	3.08	-1.80	-0.96	-0.74
ET0027	1 00 15.37	-33 39 06.2	3.10	-1.50	-0.94	-0.70
ET0028	1 00 17.77	-33 35 59.7	3.11	-1.22	-0.98	-0.78
ET0031	1 00 07.57	-33 37 03.9	2.98	-1.68	-0.88	-0.58
ET0033	1 00 20.29	-33 35 34.5	2.98	-1.77	-0.90	-0.60
ET0043	1 00 13.95	-33 36 39.2	2.84	-1.24	-1.04	-0.88
ET0048	0 59 55.63	-33 33 24.6	3.18	-1.90	-0.70	-0.24
ET0051	0 59 46.41	-33 41 23.5	3.18	-0.92	-1.12	-1.08
ET0054	0 59 56.60	-33 36 41.7	3.00	-1.81	-0.80	-0.44
ET0057	0 59 54.21	-33 40 27.2	3.02	-1.33	-0.88	-0.62
ET0059	0 59 38.11	-33 35 08.0	2.98	-1.53	-1.17	-1.13
ET0060	0 59 37.74	-33 36 00.0	2.98	-1.56	-0.94	-0.72
ET0062	0 59 47.21	-33 33 36.9	2.91	-2.27	< -0.50	< 0.00
ET0063	0 59 37.22	-33 37 10.5	2.99	-1.18	-0.96	-0.76
ET0064	0 59 41.40	-33 38 47.0	2.96	-1.38	-0.88	-0.58
ET0066	1 00 03.60	-33 39 27.1	2.94	-1.30	-1.00	-0.84
ET0067	0 59 37.00	-33 30 28.4	2.90	-1.65	-0.96	-0.72
ET0069	0 59 40.46	-33 35 53.8	2.86	-2.11	-0.82	-0.44
ET0071	0 59 58.27	-33 41 08.7	2.92	-1.35	-0.98	-0.78
ET0073	0 59 53.99	-33 37 42.1	2.82	-1.53	-0.90	-0.62
ET0083	0 59 11.83	-33 41 25.3	2.97	-1.97	-0.76	-0.34
ET0094	0 59 20.65	-33 48 56.6	3.18	-1.86	-0.82	-0.48
ET0095	0 59 20.80	-33 44 04.8	3.09	-2.16	-0.80	-0.42
ET0103	0 59 18.85	-33 42 17.3	2.95	-1.21	-1.04	-0.90
ET0104	0 59 15.14	-33 42 54.6	2.90	-1.62	-0.82	-0.46
ET0109	0 59 28.29	-33 42 07.2	3.24	-1.85	-0.76	-0.40
ET0112	0 59 52.27	-33 44 54.8	3.11	-2.04	-0.72	-0.28
ET0113	0 59 55.68	-33 46 40.1	3.08	-2.18	-0.74	-0.30
ET0121	1 00 00.49	-33 49 35.8	2.94	-2.35	-0.83	-0.43
ET0126	0 59 42.57	-33 42 18.1	2.99	-1.11	-0.96	-0.76
ET0132	0 59 58.24	-33 45 50.8	2.88	-1.50	-0.88	-0.60
ET0133	0 59 47.67	-33 47 29.5	2.88	-1.07	-1.04	-0.92
ET0137	1 00 25.30	-33 50 50.8	3.27	-0.89	-0.98	-0.82
ET0138	1 00 38.12	-33 48 16.9	3.12	-1.70	-0.92	-0.68
ET0139	1 00 42.50	-33 44 23.5	3.18	-1.41	-0.96	-0.74
ET0141	1 00 23.84	-33 42 17.4	3.08	-1.68	-0.82	-0.46
ET0145	1 00 20.75	-33 47 11.1	3.00	-1.51	-1.26	-1.30
ET0147	1 00 44.27	-33 49 18.8	3.03	-1.15	-1.24	-1.28
ET0150	1 00 22.98	-33 43 02.2	3.05	-0.93	-1.18	-1.16
ET0151	1 00 18.29	-33 42 12.2	2.98	-1.77	-0.86	-0.54
ET0158	1 00 18.96	-33 45 14.8	2.85	-1.80	-0.96	-0.74
ET0160	1 00 22.33	-33 50 24.0	2.90	-1.16	-1.00	-0.82
ET0163	1 00 24.63	-33 44 28.9	2.82	-1.86	< -0.70	< -0.40
ET0164	1 00 33.86	-33 44 54.4	2.82	-1.89	-1.08	-0.96
ET0165	1 00 11.79	-33 42 16.9	2.88	-1.10	-0.92	-0.70
ET0166	1 00 10.49	-33 49 36.9	2.83	-1.49	-0.90	-0.62
ET0168	1 00 34.32	-33 49 52.9	2.83	-1.10	-1.10	-1.00
ET0173	1 00 50.87	-33 45 05.2	3.23	-1.47	-0.84	-0.54
ET0198	1 00 09.18	-33 36 09.4	2.78	-1.16	-1.11	-1.05
ET0200	1 00 14.81	-33 36 49.9	2.77	-1.49	-0.96	-0.74
ET0202	1 00 21.08	-33 33 46.4	2.72	-1.32	-1.04	-0.88
ET0206	1 00 10.38	-33 41 05.0	2.72	-1.33	-0.98	-0.78
ET0232	0 59 54.47	-33 37 53.4	2.80	-1.00	-1.19	-1.17
ET0236	0 59 30.44	-33 36 05.0	2.74	-2.41	< -0.30	< 0.40
ET0237	0 59 50.78	-33 31 47.1	2.75	-1.61	-0.90	-0.62

Table 6. continued.

Star	RA	DEC	$\log L_*/L_\odot$	[Fe/H]	[C/Fe] _{est}	[C/Fe] _{lim}
ET0238	0 59 57.60	-33 38 32.5	2.78	-1.57	-1.00	-0.80
ET0239	0 59 30.49	-33 39 04.0	2.71	-2.26	< -0.40	< 0.30
ET0240	0 59 58.31	-33 34 40.4	2.77	-1.15	-1.02	-0.84
ET0241	1 00 02.69	-33 30 25.3	2.79	-1.41	-0.94	-0.70
ET0242	1 00 02.23	-33 40 21.1	2.86	-1.32	-0.94	-0.70
ET0244	0 59 59.65	-33 39 31.9	2.73	-1.24	-1.04	-0.90
ET0275	0 59 15.13	-33 39 43.8	2.70	-1.21	-1.08	-0.98
ET0299	0 59 08.60	-33 42 29.4	2.70	-1.83	-0.66	-0.14
ET0300	0 59 22.12	-33 49 03.7	2.75	-1.39	-0.98	-0.78
ET0317	0 59 49.91	-33 44 05.0	2.81	-1.69	-0.96	-0.74
ET0320	0 59 45.31	-33 43 53.8	2.76	-1.71	< -0.90	< -0.40
ET0321	1 00 06.98	-33 47 09.7	2.78	-1.93	-1.10	-1.00
ET0322	1 00 05.93	-33 45 56.5	2.74	-2.04	< -0.60	< 0.00
ET0327	0 59 37.56	-33 43 33.5	2.76	-1.32	-0.94	-0.68
ET0330	1 00 04.16	-33 43 32.4	2.68	-2.00	-0.68	-0.18
ET0339	0 59 44.90	-33 44 35.1	2.72	-1.08	-1.19	-1.17
ET0342	0 59 35.02	-33 50 55.9	2.62	-1.35	-1.11	-1.03
ET0350	0 59 41.95	-33 45 03.7	2.56	-1.90	< -0.50	< 0.10
ET0354	0 59 55.87	-33 45 43.7	2.56	-1.07	-1.15	-1.09
ET0363	0 59 53.08	-33 43 58.5	2.52	-1.28	-1.06	-0.94
ET0369	1 00 11.73	-33 44 50.4	2.80	-2.35	-0.81	-0.43
ET0373	1 00 17.36	-33 43 59.6	2.74	-1.96	-0.88	-0.56
ET0376	1 00 15.18	-33 43 11.0	2.78	-1.17	-0.96	-0.74
ET0378	1 00 21.17	-33 46 01.3	2.77	-1.18	-0.96	-0.76
ET0379	1 00 14.58	-33 47 11.6	2.72	-1.65	-1.11	-1.03
ET0382	1 00 17.60	-33 46 55.2	2.72	-1.74	-1.04	-0.86
ET0384	1 00 26.29	-33 44 45.7	2.71	-1.46	-1.10	-1.00
ET0389	1 00 12.52	-33 43 01.3	2.68	-1.60	-0.98	-0.78
ET0392	1 00 25.04	-33 42 28.1	2.67	-1.48	-0.86	-0.52